Supplemental information to Sea salt reactivity over the northwest Atlantic: An in-depth look using the airborne ACTIVATE dataset

Eva-Lou Edwards[1], Yonghoon Choi[2,3], Ewan C. Crosbie[2,3], Joshua P. DiGangi[2], Glenn S. Diskin[2], Claire E. Robinson[2,3,†], Michael A. Shook[2], Edward L. Winstead[2,3], Luke D. Ziemba[2], and Armin Sorooshian[1,4]

[1]Department of Chemical and Environmental Engineering, University of Arizona, Tucson, AZ, 85721, USA
[2]NASA Langley Research Center, Hampton, VA, 23681, USA
[3]Analytical Mechanics Associates, Inc., Hampton, VA, 23666, USA
[4]Department of Hydrology and Atmospheric Sciences, University of Arizona, Tucson, AZ, 85721, USA

[†]Deceased

[*]Corresponding author: armin@arizona.edu

S1. Additional information for Equations 1 - 5

Equations 1 – 4 comprise a system of four equations for determining the contribution of sea salt and dust to bulk PILS Na^+ and Ca^{2+} mass concentrations. Equation 5 (derived from Eqs. 1 – 4) can produce negative values for $ssNa^+$ depending on Na^+_{bulk} and Ca^{2+}_{bulk}. In these cases, $ssNa^+$ is set to 0, which prevents negative mass concentrations from also being assigned to Na^+_{dust}, $ssCa^{2+}$, and Ca^{2+}_{dust}.

S2. Additional information for Equations 6 - 14

Equations 6 – 13 constitute a system of equations for determining the contribution of sea salt, dust, and emissions from combustion processes to bulk PILS Na^+, Ca^{2+}, and K^+ mass concentrations. When a computer-based solver attempts to solve Eqs. 6 – 13, nonphysical results are often produced (i.e., either negative mass concentrations arise for certain species or there is no solution at all). Thus, we manually solve for one unknown variable at a time and adjust calculated values as necessary to arrive at a physical solution using the following method:

1. Manual calculations begin with Eq. 14 (derived from Eqs. 6 – 13), yet Eq. 14 can produce negative values for $ssNa^+$ depending on Na^+_{bulk}, Ca^{2+}_{bulk}, K^+_{bulk}, and the selected $\left(\frac{Na^+}{K^+}\right)_{comb}$. In these cases, $ssNa^+$ is set to 0, which prevents negative mass concentrations from also being assigned to $ssCa^{2+}$ and ssK^+ via Eq. 9 and 11, respectively.
2. If $ssCa^{2+}$ and ssK^+ exceed Ca^{2+}_{bulk} and K^+_{bulk}, respectively, $ssCa^{2+}$ and ssK^+ are set to Ca^{2+}_{bulk} and K^+_{bulk}, respectively.
3. If the sum of K^+_{dust} and ssK^+ exceed K^+_{bulk}, K^+_{dust} is set to $K^+_{bulk} - ssK^+$, which forces K^+_{comb} to be 0.
4. If the sum of Na^+_{comb} and $ssNa^+$ exceed Na^+_{bulk}, Na^+_{comb} is set to $Na^+_{bulk} - ssNa^+$, which forces Na^+_{dust} to be 0. Note that this adjustment prioritizes allotment of Na^+_{bulk} to Na^+_{comb} over Na^+_{dust}. We performed this same adjustment except prioritizing assignment of Na^+_{bulk} to Na^+_{dust} over Na^+_{comb}, and it did not significantly alter our results.

Table S1. Nomenclature for variables used in calculations relevant to Cl^- depletion.

Variable(s)	Description
$Na^+_{bulk}, Ca^{2+}_{bulk}, K^+_{bulk}, SO^{2-}_{4,\,bulk}, NO^-_{3,bulk}, oxalate_{bulk}, Cl^-_{bulk}$	Raw mass concentrations for each of the species listed from PILS-IC analysis.[1]
$NH^+_{4,bulk}$	Raw mass concentrations of NH_4^+ from the AMS[2].
$ssNa^+, ssCa^{2+}, ssK^+$	Derived mass concentrations attributed to sea salt for each of the species listed.
$Na^+_{dust}, Ca^{2+}_{dust}, K^+_{dust}$	Derived mass concentrations attributed to dust for each of the species listed.
Na^+_{comb}, K^+_{comb}	Derived mass concentrations attributed to combustion processes for each of the species listed.
$Sea\ salt$	Derived mass concentrations of sea salt.
$\%Cl^-\ depletion$	Derived percentages of the original Cl^- in sea salt particles that has since been displaced through depletion reactions.
$Lost\ Cl^-$	Derived mass concentrations of particulate Cl^- displaced from sea salt particles (when reported in units of μg m^{-3}) or the molar fraction of gaseous Cl added to the atmosphere following Cl^- depletion reactions (when reported in units of pptv or ppbv). Note these are equivalent. Values are calculated using Approach 1, meaning that non-sea salt sources of Na^+ are considered.
$Lost\ Cl^-_{bulk}$	Same as lost Cl^- above, but calculated using Approach 2, meaning that sea salt is assumed to be the only source of atmospheric Na^+.
$Lost\ Cl^-_{diff}$	Difference between lost Cl^-_{bulk} and lost Cl^-, which is used to understand how assumptions about the source(s) of atmospheric Na^+ affect derived amounts of displaced Cl^-.
$nssSO^{2-}_4$	Derived mass concentrations of SO_4^{2-} attributed to sources other than sea salt.
$ExSO^{2-}_4, ExNO^-_3$	Derived mass concentrations of SO_4^{2-} and NO_3^-, respectively, remaining after neutralization with NH_4^+.
$ExNH^+_4$	Derived mass concentrations of remaining NH_4^+ after neutralizing $nssSO_4^{2-}$.
$Excess\ acidic\ species$	Derived total mass concentrations of the acidic species not neutralized by ammonium and, thus, having the potential to displace Cl^- from sea salt particles.
$Lost\ Cl^-\ attr.\ to\ A$	Hypothetical mass concentrations of the amount of Cl^- a given acidic species has the potential to displace, where A can be $ExSO_4^{2-}$, Ex NO_3^-, or $oxalate_{bulk}$.
$Lost\ Cl^-\ attr.\ to$ excess acidic species	Hypothetical mass concentration of the total Cl^- that can be displaced from sea salt particles based on the available amount of excess acidic species.

[1]"PILS-IC analysis" refers to in-flight sampling with a particle into liquid sampler (PILS) following by offline sample analysis using ion chromatography (IC).

[2]"AMS" stands for aerosol mass spectrometer.

Table S2. Mass ratios, molecular weights, and charges of fully deprotonated conjugate bases used in calculations relevant to Cl^- depletion.

Type of parameter	Parameter	Value
Mass ratio [unitless]	$\left(\frac{total\ mass}{Na^+}\right)_{ss}$	3.267[a]
	$\left(\frac{Ca^{2+}}{Na^+}\right)_{ss}$	0.038[b, c]
	$\left(\frac{Ca^{2+}}{Na^+}\right)_{dust}$	1.78[b]
	$\left(\frac{K^+}{Na^+}\right)_{ss}$	0.036[a, c]
	$\left(\frac{K^+}{Ca^{2+}}\right)_{dust}$	1.00[d]
	$\left(\frac{Na^+}{K^+}\right)_{comb}$	See Table S2
	$\left(\frac{SO_4^{2-}}{Na^+}\right)_{ss}$	0.253[e, f, g]
	$\left(\frac{Cl^-}{Na^+}\right)_{ss}$	1.81[b]
Molecular weight [g mol^{-1}]	$MW_{SO_4^{2-}}$	96.056
	$MW_{NH_4^+}$	18.039
	$MW_{NO_3^-}$	62.005
	MW_{Cl^-}	35.453
	$MW_{oxalate}$	88.019
Charge of fully deprotonated conjugate base [unitless]	$y_{SO_4^{2-}}$	2
	$y_{NO_3^-}$	1
	$y_{oxalate}$	2

[a]Seinfeld and Pandis (2016)
[b]Bowen (1979)
[c]Finlayson-Pitts and Pitts (2000)
[d]Aldhaif et al. (2020)
[e]Becagli et al. (2005)
[f]Boreddy and Kawamura (2015)
[g]Farren et al. (2019)

Table S3. Details regarding the various $\left(\frac{Na^+}{K^+}\right)_{comb}$ ratios used when exploring how different combustion processes may affect calculations relevant to Cl^- depletion.

Indicator used in text	Description of combustion process	Value
Herbaceous agricultural fire	Agricultural burning of herbaceous crop residue	0.05[a]
Forest fire	Forest fire burning of pinion and juniper trees	0.08[b]
Industrial (avg)	Average from industrial operations at steel mills and cement plants	0.24[c, d]
Sauna stove	Inefficient batch combustion of birch wood in a sauna stove for residential heating	0.75[e]
Car exhaust	Fossil fuel combustion by motor vehicles	0.91[c, f]
Coal combustion (avg)	Average from burning of pulverized western coal comprised of low sulfur (0.5%) and high ash (22%) at a coal-fired power plant	3.03[c, g]

[a]Turn et al. (1997)
[b]Watson et al. (2001)
[c]Ooki et al. (2002)
[d]Scheff and Valiozis (1990)
[e]Lamberg et al. (2011)
[f]Huang et al. (1994)
[g]Ondov et al. (1989)

Table S4. Summary of findings from this work as well as those from previous studies conducted around the globe. "BDL" stands for below detection limit, and "SSA" stands for sea salt aerosol. Several abbreviations are used and are defined as the following: "Ref" = reference, "Alt" = relevant altitudes, "Dp" = particle size range, "Stat" = statistic reported, "SSA" = sea salt aerosol, "Attr. Na^+ to nss sources" = Attributes Na^+ to non-sea salt sources, "Eq" = equation, "Air" = aircraft, "Surf" = surface station(s), "Med" = median, and "Rng" = range, "USEC" = United States East Coast, and "BDL" = below detection limit.

Ref	Date	Site	Platform	Alt	D_p	Stat	SSA	Na^+	K^+	Ca^{2+}	Cl^-	Nss SO_4^{2-}	NO_3^-	NH_4^+	Cl^-: Na^+	Lost Cl^-	Cl^- depletion	Attr. Na^+ to nss sources	Eq/ method for determining SSA mass and/or Cl^- depletion (%)	Eq/ method ref
				m a.s.l	µm		µg m^{-3}	µg m^{-3}	µg m^{-3}	µg m^{-3}	µg m^{-3}	µg m^{-3}	µg m^{-3}	µg m^{-3}		µg m^{-3}/ pptv	%			
This study	Dec-Feb 2022	USEC; 34.0°–41.7° N/ 70.0°–76.7° W	Air	160 – 2000	< 5[1]	Med	0.61	0.25	0.04	0.06	0.32	0.66	0.49	0.27	1.70[2]	0.04/27	6	Yes	Eqs. 1 – 4, 15, 16	Boreddy and Kawamura (2015); AzadiAghdam et al. (2019)
	Mar 2022	USEC; 32.2°–38.5° N/ 69.1°–76.5° W					0.65	0.27	0.07	0.13	0.43	0.71	0.81	0.38	1.62[2]	0.04/27	10			
	May 2022	USEC; 32.3°–41.7° N/ 69.1°–76.5° W					0.95	0.26	0.05	0.12	0.46	0.90	0.55	0.57	0.64[2]	1.76/ 1174	64			
	Jun 2022	Bermuda; 30.8°–35.9° N/ 59.5°–65.9° W					4.3	1.24	0.06	0.07	1.68	1.34	0.90	0.22	1.35[2]	0.66/440	25			
Studies in open ocean environments																				
Prospero (1979)	Jun-Aug 1975	NWA; 34°–40° N/ 52°–60° W	Ship	15	< 30	Mean	4.41[3] / 5.52[4]											No	$SSA = 3.252 \cdot Na^+$	
Spada et al. (2015)	1987 - 1996	New Zealand; 41.3°–46.4° S/ 168.4° E–176.5° W	Surf		No upper limit	Rng	~6 - 14											No	$SSA = 1.47 \cdot Na^+ + Cl^-$	Quinn and Bates (2005)
Keene et al. (1990)	Jul-Sep 1988	Bermuda	Ship	10-m tower on ship	No upper limit	Mean					1.33					0.68/454			Multiplies Na^+ by ratio in seawater	

			Air	MBL						0.13					0.34/227				
Heintzenberg et al. (2000)	1990-1997	30°-45° N[5]	Ship and air	MBL	N/A	Mean	~6				~3						No	$SSA = 3.262 \cdot Na^+$	Wilson (1975)
Shinozuka et al. (2004)	Nov-Dec 1995	Tasmania; 135°-160° E/38°-57° S	Air	< 2000	< 3.5/ No upper limit[6]	Rng	0 – 8/ 9 - 40										No	$SSA = 1.47 \cdot Na^+ + Cl^-$	Holland (1978); Quinn et al. (2001)
Keene and Savoie (1998)	Apr-May 1996	Bermuda; 32° N/64° W	Surf	28	0.55-17	Rng				3.42 – 8.26		0.10 – 1.36[6]			0.22 – 1.35/147 – 900		No	$SSA = 3.262 \cdot Na^+$	Keene et al. (1986); Wilson (1975)
Quinn and Bates (2005)	Nov-Dec 1995	Southern Ocean south of Australia	Ship	18	< 10	Mean	0.77		BDL		0.03	BDL	0.01				No	$SSA = 1.47 \cdot Na^+ + Cl^-$	
	Jun-Jul 1997	Sub-tropical northeast Atlantic					0.30		BDL		0.20	0.08	0.03						
	Jan-Feb 1999	Tropical Atlantic					0.38 /0.43[8]		BDL/ 0.01[8]		0.01/ 0.08[8]	0.02/ 0.06[8]	0.00/ 0.01[8]						
Quinn et al. (2001)	Jan-Feb 1999	Northern hemisphere marine[9]	Ship	18	< 1.1/ 1.1 – 10	Mean	0.22/ 8.00		0.00/ 0.01		0.15/ <0.00	0.01/ 0.23	0.03/ <0.00				No	$SSA = 1.47 \cdot Na^+ + Cl^-$	Holland (1978)
		Southern hemisphere marine tropics[9]					0.08/ 6.40		0.00/ 0.00		0.52/ 0.07	<0.00 / 0.19	0.05/ <0.00						
		Southern hemisphere marine temperate[9]					0.14/ 9.5		0.00/ 0.00		0.56/ 0.03	<0.00 /0.14	0.04/ <0.00						
Boreddy and Kawamura (2015)	Dec-Feb 2001-2012	Chichijima Island; 27.1 °N /142.2 °E	Surf	259	No upper limit	Mean		4.12	0.05^{10}	0.12^{10}	7.10	3.06	0.78	0.19	1.75		Yes	Same system of equations as Eqs. 1-4 in this study	
	Mar-May 2001-2012							3.32	0.05^{10}	0.30^{10}	6.18	2.97	0.84	0.23	1.67				

	Jun-Aug 2001-2012							2.52	0.02[10][1]	0.04[10]	4.94	1.06	0.24	0.11	1.82[11][1]						
	Sep-Nov 2001-2012							3.62	0.05[10][1]	0.04[10]	7.12	1.31	0.43	0.11	1.98[11][1]						
Jiang et al. (2021)	Summer 2008-2016	Northwest Pacific; 31°–51.3° N/ 122°–173° E	Ship	Top deck of ship	Unspecified	Rng (Mean)	1.6 – 42.0 (11.7)											No	$SSA = 3.256 \cdot Na^+$	Riley and Chester (1976)
Feng et al. (2017)	Nov 2012/ 2013	Yellow Sea and Bohai Sea	Ship		0.01-18	Mean	3.8/4.0										8% and 35% for particles < 10 and < 1 μm, respectively	No	$SSA = 3.26 \cdot Na^+$	Manders et al. (2010)
	Mar-Apr 2014	Yellow Sea and North Pacific					4.0													
	Mar-May 2015						2.5													
Murphy et al. (2019)	Jul-Aug 2016, Jan-Feb 2017	30°–45° N over Pacific Ocean	Air	160-1500	0.18-3	Rng	~0.5 – 2.5											Yes[12]	Method using ion mass spectra	
Studies in coastal locations																				
Keene et al. (1990)	Jul-Sep 1988	USEC	Ship	10-m tower on ship	No upper limit	Mean					4.04					1.11/740		No	Multiplies Na^+ by ratio in seawater	
			Air	MBL							0.45					0.79/527				

Wai and Tanner (2004)	1995 - 1999	Hong Kong; 22.3° N/114.1 ° E	Surf	77	< 10	1995 mean	2.32										Yes[13]	Uses Na^+ as indicator of SSA	
Quinn et al. (2001)	Jan-Feb 1999	USEC[8]	Ship	18	< 1.1/ 1.1 - 10	Mean	0.12/ 9.20		0.02/ <0.00		2.40/ 0.09	0.04/ 2.30	0.54/ <0.00				No	$SSA = 1.47 \cdot Na^+ + Cl^-$	Holland (1978)
Quinn and Bates (2005)	Jan-Mar 1999	Northern Indian Ocean	Ship	18	< 10	Means	0.25/ 0.08[14]		BDL/ 0.01[14]		0.05/ 0.25[14]	0.04/ 0.07[14]	0.01/ 0.05[14]					$SSA = 1.47 \cdot Na^+ + Cl^-$	
	Mar-Apr 2001	East coast of Japan, Sea of Japan, East China Sea					0.08/ 0.06[15]		BDL/ BDL[15]		0.15/ 0.07[15]	0.07/ 0.03[15]	0.05/ 0.02[15]						
	Jul-Aug 2002	USEC; 33°-45° N					0.04		BDL	0.17		0.03	0.05	0.4 (< 1 µm)/ 0.8 (1 - 10 µm)						
Keene et al. (2004)	Jul-Aug 2002	USEC; 33°-44° N/ 68°-80° W	Ship	18	<25	Median				0.19	3.48	0.79	0.57			86	N/A	Uses Mg^{2+} as reference for SSA	Keene et al. (1986)
Nolte et al. (2008)	May-Jun 2002	Tampa, Florida, USA; ~27.9° N,82.5° W	Surf	Unspecified	0.056 - 18	Mean or rng		1.41		1.66	3.76[16]	1.74	1.19	0.2 – 0.35 (< 1 µm)/ 0.35 - 0.9 (> 1 µm)		48	No	Cl^- depletion (%) determined by deficit of Cl^-/Na^+ ratio from 1.17	Stumm and Morgan (1981)
Yao and Zhang (2012)	Jun-Jul, Oct-Nov 2002	Kejimkujik, Nova Scotia; 44.4° N /65.2° W	Surf	5 m above ground	3.1 – 6.2	Rng summer/ fall		0.05 – 0.22/ 0.03 – 0.24								8 – 100/ 0 - 55	No	Uses Cl^-:Na^+ ratio of 1.174 in sea water to determine Cl^- depletion (%)	Zhuang et al. (1999)
	Nov 2002[17]				0.048 - 18	Rng <1 µm /> 1 µm		BDL – 0.07/ 0.72 – 1.59			1.04 – 2.92/ 0.11 – 2.33	0.02 – 0.18/ 0.69 – 2.35	0.31 – 0.91/ 0.02 – 0.80						
Keene et al. (2007)	Jul-Aug 2004	Appledore Island, Maine, USA;	Surf	43	0.39 – 18/ No upp	Mean or rng		0.68		0.50	0.96 – 21.61	0.26 – 1.57			0.00 – 1.31/0 - 874		No[19]	Uses Na^+ and Mg^{2+} to determine SSA	Keene et al. (1986)

		42.9° N/70.6° W			er limit[18]															
Zhao and Gao (2008)	Jul-Sep 2006	Newark, New Jersey, USA; 40.7° N/74.2° W	Surf	20 m above ground	0.056 – 18	Mean or rng									0.33 – 1.21		14 - 96	Yes[20]	For samples with Na^+:Mg^{2+} >5 , Na^+ is reference species for SSA	Finlayson-Pitts and Pitts (2000)
Corral et al. (2021)	Dec-Feb 2014 - 2018 Mar-May 2014 - 2018 Jun-Aug 2014 - 2018 Sep-Nov 2014 - 2018	USEC; 25.4°–44.4° N/70.0°–82.1° W	Surf[21]	-3 - 157	< 2.5	Rng of means across 9 stations	0.24-1.15 0.35 – 1.26 0.15 – 0.70 0.19-1.09											N/A	$SSA = 1.81 \cdot Cl^-$	http://vista.cira.colostate.edu/Improve/reconstructed-fine-mass/
Haskins et al. (2018)	Feb-Mar 2015	USEC; ~28°–43° N/68°–85° W	Air	< 1000	< 4.1	Med					Over ocean: 0.28 – 0.2 Over land: 0.12 – 0.15[22]					Over ocean: 0.30/202 Over land: 0.08/53		No	Na^+ and Cl^- are assumed to come exclusively from SSA	Junge and Werby (1958)
Kloppe r et al. (2020)	Feb 2016 – Dec 2017	Henties Bay, Namibia	Surf	30	< 10	Mean		10.2	0.41	0.73	13.9	3.60[23]	0.23	0.21	1.35 (2016)/ 1.34 (2017)			Yes	Similar system of equations as Eqs.1-4 in this study	Seinfeld and Pandis (2016)
Azadi Aghdam et al. (2019)	Jul-Dec 2018 Aug 2005 – Oct 2007	Quezon City, Philippines; 14.6° N/ 121.1° E	Surf	85	0.056 - 18 < 2.5 (P	Rng Rng of means	0.1 – 2.6	0.20 – 1.48				2.03 – 3.12/ 0.31	0.17 – 0.35/		0.32 – 0.59/		21 - 91	Yes	Same as Eqs. 1-4, 15, 16 in this study; $SSA = ssNa^+ + Cl^-$	Becagli et al. (2005); Boreddy and Kawamura (2015); Farren et al. (2019)

					$M_{2.5}$)/ 2.5 – 10 (PM_{coarse})			– 0.44	0.44 – 0.74	1.46 – 1.59				
Studies at inland locations														
Bondy et al. (2017)	Jun-Jul 2013	Centreville, Alabana, USA; 32.9° N/87.3° W	Surf	242	0.32 – 1.8						76 % of SSA particles had Cl- depletion ≥ 90 %	Yes[24]	Method using ion mass spectra; SSA particles identified as having Na^+:Mg^{2+} ~10:1	Pilson (1998)

[1]Median values for NH_4^+ are for particles 0.06 – 0.60 µm.
[2]Ratios of Cl^-:ssNa^+ are reported instead of Cl^-:Na^+.
[3]Geometric mean.
[4]Arithmetic mean.
[5]Heintzenberg et al. (2000) consider data from multiple field campaigns covering nearly all longitudes and latitudes (see Fig. 1 of their study) over ocean. Thus, means listed above represent the 30° – 45° N latitude band over ocean for the entire globe instead of a specific region.
[6]Filters inside the aircraft sampled particles < 3.5 µm, while filters outside the aircraft did not have an upper limit for the size of particles sampled.
[7]Ranges of NO_3^- mass concentrations are for particles > 1 µm, all other ranges are for the specified size range (0.55 – 17 µm).
[8]In the tropical Atlantic, air masses influenced by biomass burning (BB) and African dust were sampled. Mean values for a given parameter are reported as A/B, where A and B correspond to values associated with BB- and dust-influenced air masses, respectively.
[9]Regimes defined in Quinn et al. (2001). Note that ranges of longitude and latitude are not provided for these regimes, but that the research vessel traveled from Norfolk, VA, USA (36.9° N, 76.3° W) to Cape Town, South Africa (34.3° S, 18.4° E).
[10]Boreddy and Kawamura (2015) report non-sea salt K^+ and Ca^{2+}.

[11]These Cl^-:Na^+ ratios are higher than those typically found in sea salt particles. Boreddy and Kawamura (2015) note that non-sea salt sources of Cl^- contributed to their samples in summer (June – August) and fall (September – November).

[12]Particles containing aluminum, barium, and other metals were deemed to not be sea salt particles and excluded from the analysis in Murphy et al. (2019).

[13]Wai and Tanner (2004) reported they "carefully examined their dataset" and determined there was negligible contribution of local non-sea salt sources of Na^+ (e.g., crustal, granitic) to total Na^+.

[14]In the northern Indian Ocean, air masses were categorized as having recent (<2 days) contact with either the Arabian or Indian continent. Mean values for a given parameter are reported as A/B, where A and B correspond to values associated with air masses from the Arabian and Indian continent, respectively.

[15]On the east coast of Japan, Sea of Japan, and East China Sea, air masses were categorized as having recent (<2 days) contact with either (i) Asian continental regions with known sources of pollution or (ii) Asian continental regions with known sources of pollution and dust. Mean values for a given parameter are reported as A/B, where A and B correspond to values associated with air masses likely affected by (i) Asian pollution and (ii) Asian pollution and dust, respectively.

[16]Nolte et al. (2008) reported total SO_4^{2-} instead of $nssSO_4^{2-}$.

[17]Yao and Zhang (2012) provided speciated sub- and supermicron mass concentrations for three samples collected in November 2002 that had substantially high mass concentrations of Na^+, $nssSO_4^{2-}$, NO_3^-, and NH_4^+.

[18]Aerosols were sampled using a cascade impactor (0.39 – 18 μm) as well as in bulk where no upper size limit is specified. Cl^- and NO_3^- mass concentrations correspond to the sum across all impactor stages, while Na^+ and $nssSO_4^{2-}$ mass concentrations correspond to the bulk samples.

[19]Keene et al. (2007) found good agreement between their measured ratios of Na^+ to Mg^{2+} to those documented for sea salt. They proceeded assuming all Na^+ and Mg^{2+} originated from the surface ocean.

[20] Zhao and Gao (2008) used Na^+:Mg^{2+} ratios to categorize samples as either from marine-dominated (Group 1; >5) or continental-dominated (Group 2; < 5) air masses. Calculations and discussion regarding Cl^- depletion only consider data from Group 1.

[21]Stations operated through the United States Environmental Protection Agency (U.S. EPA) Interagency Monitoring of Protected Visual Environments (IMPROVE) network.

[22]Haskins et al. (2018) provided day and night median Cl^- mass concentrations for over ocean and over land. Above, we combine the day and night medians as a range.

[23]Klopper et al. (2020) reported total SO_4^{2-} instead of $nssSO_4^{2-}$.

[24]Bondy et al. (2017) note particles identified and analyzed as sea salt were unlikely to be influenced by dust as they had negligible amounts of soil elements, such as Si and Al. Samples from July 4 and 5 were excluded to eliminate influence from fireworks.

Table S5. Number of data points considered in Figs. 1, 4, and S6 for each of the parameters presented for each of the seasonal/monthly categories.

Parameter	Dec-Feb	Mar	Mar transit	May	May transit	Jun Bermuda
Temperature	105781	83108	12806	34175	27427	19807
Relative humidity	105846	83098	12805	34175	27421	19803
Water vapor mixing ratio	105846	83098	12805	34175	27421	19803
Wind speed	75483	58823	7994	19826	12955	6477
CO	75523	58407	8545	23799	18745	10946
Na^+	275	246	48	113	106	81
K^+	218	217	47	60	43	52
Ca^{2+}	235	244	48	73	81	67
Cl^-	268	230	43	43	65	78
Cl^-:Na^+	258	227	43	43	65	77
K^+:Na^+	185	208	47	58	41	52
Ca^{2+}:Na^+	202	220	48	64	75	66
SO_4^{2-}	342	276	48	136	116	81
NO_3^-	322	269	48	137	119	83
Oxalate	263	227	43	137	120	82
NH_4^+	2748	2385	403	1169	947	678
Excess acidic species	1372	1790	423	468	373	486
$ssNa^+$	202	220	48	64	75	66
Cl^-:$ssNa^+$	154	175	36	33	52	63
Lost Cl^- attributed to $ExSO_4^{2-}$	1258	1748	418	391	323	466
Lost Cl^- attributed to $ExNO_3^-$	1212	1733	418	391	323	466
Lost Cl^- attributed to oxalate	263	227	43	137	120	82
Lost Cl^- based on $ssNa^+$	190	206	43	33	53	64
Lost Cl^- attributed to excess acidic species	1385	1794	423	468	373	487
$ExSO_4^{2-}$	1258	1748	418	391	323	466
$ExNO_3^-$	1212	1733	418	391	323	466
m/z 44	2748	2385	403	1169	947	678
m/z 79	2748	2385	403	1169	947	678

Table S6. Seasonal/monthly median values for each of the parameters presented in Figs. 1, 4, and S6. Recall the median is represented as a solid red line in the center of each box.

Parameter	Units	Dec-Feb	Mar	Mar transit	May	May transit	Jun Bermuda
Temperature	°C	2.7	9.2	13.3	19.9	19.2	21.9
Relative humidity	%	52.6	50.5	46.6	64.2	61.6	80.8
Water vapor mixing ratio	ppm	3607.38	5585.31	6868.43	15798.90	15681.40	21605.40
Wind speed	m s^{-1}	8.926	10.266	8.617	8.355	6.710	6.425
CO	ppm	0.1332	0.1404	0.1408	0.1246	0.1214	0.0813
Na^+	µg m^{-3}	0.25	0.27	0.75	0.26	0.46	1.24
K^+		0.04	0.07	0.09	0.05	0.03	0.06
Ca^{2+}		0.06	0.13	0.14	0.12	0.05	0.07
Cl^-		0.32	0.43	1.33	0.46	0.31	1.68
Cl^-:Na^+	-	1.443	1.309	1.376	0.391	0.456	1.310
K^+:Na^+		0.132	0.267	0.119	0.065	0.020	0.037
Ca^{2+}:Na^+		0.261	0.412	0.219	0.233	0.075	0.050
SO_4^{2-}	µg m^{-3}	0.63	0.74	1.08	0.53	0.72	1.63
NO_3^-		0.49	0.81	0.77	0.55	0.74	0.90
Oxalate		0.01	0.01	0.01	0.04	0.03	0.02
NH_4^+		0.28	0.38	0.46	0.58	0.56	0.24
Excess acidic species		0.30	0.57	0.36	0.05	0.44	1.82
$ssNa^+$		0.19	0.20	0.71	0.29	0.63	1.32
Cl^-:$ssNa^+$	-	1.536	1.560	1.617	0.645	0.471	1.354
Lost Cl^- attributed to $ExSO_4^{2-}$	µg m^{-3}	0.00	0.00	0.00	0.00	0.00	0.46
Lost Cl^- attributed to $ExNO_3^-$		0.13	0.29	0.18	0.00	0.42	0.58
Lost Cl^- attributed to oxalate		0.01	0.01	0.01	0.03	0.03	0.02
Lost Cl^- based on $ssNa^+$		0.04	0.04	0.11	1.76	1.33	0.66
Lost Cl^- attributed to excess acidic species		0.17	0.34	0.21	0.04	0.26	1.14
$ExSO_4^{2-}$		0.00	0.00	0.00	0.00	0.00	0.63
$ExNO_3^-$		0.24	0.51	0.32	0.00	0.74	1.02
m/z 44		0.11	0.22	0.38	0.46	0.41	0.03
m/z 79		0.01	0.02	0.03	0.03	0.02	0.01

Table S7. Dates, quantity of samples, meteorological conditions, and derived contributions of sea salt and dust to bulk PILS Na^+ ($ssNa^+$ and Na^+_{dust}, respectively) and Ca^{2+} ($ssCa^{2+}$ and Ca^{2+}_{dust}, respectively) mass concentrations for research flights (RFs) considered in each category. "N PILS samples" refers to the total number of PILS samples collected during clear conditions on the date indicated, while "N samples w/ derived species" refers to the number of these samples providing enough information to solve Eqs. 1 – 4 (i.e., samples providing mass concentrations of both Na^+_{bulk} and Ca^{2+}_{bulk}).

Category	Date	RF(s)	N PILS samples	N samples w/ derived species	Meteorological conditions and/or relevant notes	Median $ssNa^+$ ($\mu g\ m^{-3}$)	Median Na^+_{dust} ($\mu g\ m^{-3}$)	Median $ssCa^{2+}$ ($\mu g\ m^{-3}$)	Median Ca^{2+}_{dust} ($\mu g\ m^{-3}$)
Dec-Feb	30 November 2021	94	7	7	Remains of post-frontal conditions	0.00	0.14	0.00	0.31
	01 December 2021	95	16	16	Prefrontal, high pressure; smoke in boundary layer near coast	0.03	0.23	0.00	0.47
	07 December 2021	96	5	5	Postfrontal, cold high pressure behind a strong cold front	0.07	0.11	0.00	0.20
	11 January 2022	100, 101	6	4	Cold high pressure, cold air outbreak (CAO) conditions	0.32	0.03	0.01	0.07
	12 January 2022	102, 103	33	17	Cold high pressure	0.09	0.01	0.00	0.03
	15 January 2022	104	3	2	Postfrontal	0.67	0.02	0.01	0.04
	18 January 2022	105	11	0	Low pressure moves offshore, sets up CAO conditions	NaN	NaN	NaN	NaN
	19 January 2022	107, 108	26	6	Short-lived high pressure	0.28	0.04	0.01	0.07
	24 January 2022	109, 110	26	9	Postfrontal, weak high pressure	0.16	0.04	0.00	0.07
	26 January 2022	111, 112	20	7	Postfrontal	0.35	0.02	0.01	0.04
	27 January 2022	113, 114	18	5	Cold high pressure	0.24	0.00	0.01	0.00
	01 February 2022	115	8	5	High pressure	1.07	0.01	0.03	0.03

	02 February 2022	116	17	6	High pressure	0.74	0.00	0.02	0.01
	03 February 2022	117, 118	15	5	High pressure	1.00	0.00	0.02	0.00
	15 February 2022	120, 121	34	21	Postfrontal conditions, cold high pressure	0.22	0.01	0.00	0.02
	16 February 2022	122, 123	21	18	Cold high pressure	0.17	0.04	0.01	0.08
	19 February 2022	124, 125	38	30	Weak postfrontal	0.09	0.02	0.00	0.05
	22 February 2022	126, 127	25	24	Prefrontal, high pressure	1.47	0.03	0.04	0.05
	26 February 2022	128, 129	16	15	Postfrontal	0.11	0.03	0.00	0.05
	Overall		**345**	**202**		**0.19**	**0.03**	**0.01**	**0.06**
Mar	02 March 2022	130	39	36	Postfrontal, high pressure	0.19	0.08	0.01	0.15
	03 March 2022	131, 132	71	57	Weak prefrontal	0.71	0.13	0.03	0.26
	04 March 2022	133, 134	42	37	Cold high pressure	1.62	0.02	0.04	0.04
	13 March 2022	138	8	6	Postfrontal, CAO conditions	0.05	0.03	0.00	0.06
	14 March 2022	139, 140	38	36	Late postfrontal, cold high pressure; smoke plume sampled from a woodland fire	0.10	0.03	0.00	0.05
	18 March 2022	141	14	12	Weak postfrontal	0.13	0.02	0.00	0.03
	26 March 2022	144, 145	29	19	Postfrontal; sampled dust, smoke, and potentially pollen	0.02	0.02	0.00	0.04
	28 March 2022	146	17	12	Postfrontal	0.02	0.02	0.00	0.04
	29 March 2022	147, 148	19	5	Postfrontal, high pressure, CAO conditions	0.06	0.03	0.00	0.05

May	**Overall**		**277**	**220**		**0.20**	**0.05**	**0.01**	**0.11**
	03 May 2022	149	15	12	Weak prefrontal; presence of smoke potentially from New Mexico	0.36	0.07	0.01	0.13
	05 May 2022	150, 151	18	11	Postfrontal	0.03	0.02	0.00	0.04
	16 May 2022	153, 154	39	7	Prefrontal to an approaching cold front yet also postfrontal to a departing band of precipitation	0.11	0.14	0.00	0.26
	17 May 2022	155	37	7	Postfrontal	0.08	0.00	0.00	0.00
	20 May 2022	158	28	27	Warm high pressure, southerly flow due to Bermuda high[2]; haze with potential sampling of bioaerosol	1.77	0.04	0.06	0.08
	Overall		**137**	**64**		**0.29**	**0.03**	**0.01**	**0.07**
Mar transit	22 March 2022	142, 143	48	48	High pressure, two days after a cold front and two days before another cold front	0.71	0.05	0.03	0.10
May transit	18 May 2022	156, 157	67	46	Postfrontal along East Coast, aircraft passed across the cold front on the way to Bermuda	0.58	0.01	0.02	0.02
	21 May 2022	159, 160	42	24	Warm high pressure, anticyclonic flow around Bermuda high	0.72	0.01	0.02	0.02
	31 May 2022	161	11	5	Postfrontal	0.19	0.01	0.01	0.02
	Overall		**120**	**75**		**0.63**	**0.01**	**0.02**	**0.02**
Jun Bermuda	02 June 2022	162, 163	4	3	Prefrontal	0.83	0.00	0.01	0.00
	03 June 2022	164	1	0	Prefrontal, tropical system approaching from the southwest	NaN	NaN	NaN	NaN
	05 June 2022	165	29	26	Could only fly in the morning due to approaching tropical cyclone (TC), TC departs 06 June 2022.	1.94	0.00	0.07	0.00
	07 June 2022	167	1	0	High behind departing TC	NaN	NaN	NaN	NaN
	08 June 2022	168, 169	2	1	High pressure behind TC, African dust known to be in domain	5.63	0.48	0.21	0.86
	10 June 2022	170	1	1	High pressure, isolated thunderstorms, African dust known to be in domain	2.28	0.00	0.06	0.00

	11 June 2022	172, 173	20	12	High pressure, African dust known to be in domain	0.63	0.08	0.02	0.18
	13 June 2022	174	25	23	High pressure, African dust known to be in domain but sampled away from dust for contrast	1.31	0.00	0.05	0.01
	Overall		**83**	**66**		**1.32**	**0.01**	**0.05**	**0.01**

[1]Davis et al. (1997)

Table S8. Dates, quantity of samples, meteorological conditions, and derived contributions of sea salt, dust, and combustion emissions to bulk PILS Na^+ ($ssNa^+$, Na^+_{dust}, and Na^+_{comb}, respectively) and K^+ (ssK^+, K^+_{dust}, and K^+_{comb}, respectively) for RFs considered in each category. Combustion emissions are assumed to not be a source of Ca^{2+}, so only contributions of sea salt and dust to bulk PILS Ca^{2+} mass concentrations are reported ($ssCa^{2+}$ and Ca^{2+}_{dust}, respectively). Here, agricultural burning of herbaceous crop residue is considered as the only combustion process contributing to Na^+_{comb} and K^+_{comb}. "N PILS samples" refers to the total number of PILS samples collected during clear conditions on the date indicated, while "N samples w/ derived species" refers to the number of these samples providing enough information to solve Eqs. 6 – 13 (i.e., samples providing mass concentrations of Na^+_{bulk}, Ca^{2+}_{bulk}, and K^+_{bulk}).

Category	Date	RF(s)	N PILS samples	N samples w/ derived species	Meteorological conditions and/or relevant notes	Median $ssNa^+$ ($\mu g\ m^{-3}$)	Median Na^+_{dust} ($\mu g\ m^{-3}$)	Median Na^+_{comb} ($\mu g\ m^{-3}$)	Median $ssCa^{2+}$ ($\mu g\ m^{-3}$)	Median Ca^{2+}_{dust} ($\mu g\ m^{-3}$)	Median ssK^+ ($\mu g\ m^{-3}$)	Median K^+_{dust} ($\mu g\ m^{-3}$)	Median K^+_{comb} ($\mu g\ m^{-3}$)
Dec-Feb	30 November 2021	94	7	1	Remains of post-frontal conditions	0.00	0.16	0.00	0.00	0.41	0.00	0.06	0.00
	01 December 2021	95	16	14	Prefrontal, high pressure; smoke in boundary layer near coast	0.08	0.23	0.00	0.00	0.48	0.00	0.05	0.00
	07 December 2021	96	5	3	Postfrontal, cold high pressure behind a strong cold front	0.08	0.11	0.00	0.00	0.22	0.00	0.03	0.00
	11 January 2022	100, 101	6	3	Cold high pressure, cold air outbreak (CAO) conditions	0.33	0.03	0.00	0.01	0.08	0.01	0.01	0.00
	12 January 2022	102, 103	33	11	Cold high pressure	0.15	0.04	0.00	0.01	0.08	0.00	0.02	0.00
	15 January 2022	104	3	2	Postfrontal	0.67	0.02	0.00	0.01	0.04	0.01	0.00	0.00
	18 January 2022	105	11	0	Low pressure moves offshore, sets up CAO conditions	NaN	NaN	NaN	NaN	NaN	NaN	NaN	NaN
	19 January 2022	107, 108	26	6	Short-lived high pressure	0.28	0.04	0.00	0.01	0.07	0.01	0.05	0.06
	24 January 2022	109, 110	26	9	Postfrontal, weak high pressure	0.17	0.04	0.00	0.00	0.07	0.01	0.05	0.02
	26 January 2022	111, 112	20	7	Postfrontal	0.33	0.02	0.01	0.01	0.04	0.01	0.03	0.35

	27 January 2022	113, 114	18	4	Cold high pressure	0.28	0.00	0.00	0.01	0.00	0.01	0.00	0.00
	01 February 2022	115	8	4	High pressure	1.08	0.01	0.00	0.02	0.03	0.02	0.00	0.00
	02 February 2022	116	17	4	High pressure	0.74	0.00	0.00	0.02	0.01	0.03	0.00	0.02
	03 February 2022	117, 118	15	4	High pressure	1.16	0.00	0.00	0.03	0.00	0.04	0.00	0.01
	15 February 2022	120, 121	34	7	Postfrontal conditions, cold high pressure	0.11	0.04	0.00	0.00	0.13	0.00	0.02	0.00
	16 February 2022	122, 123	21	10	Cold high pressure	0.13	0.06	0.00	0.00	0.12	0.00	0.04	0.00
	19 February 2022	124, 125	38	18	Weak postfrontal	0.06	0.02	0.00	0.00	0.11	0.00	0.04	0.00
	22 February 2022	126, 127	25	20	Prefrontal, high pressure	1.68	0.03	0.00	0.04	0.07	0.04	0.00	0.00
	26 February 2022	128, 129	16	14	Postfrontal	0.10	0.02	0.00	0.00	0.05	0.00	0.04	0.00
	Overall		**345**	**141**		**0.21**	**0.03**	**0.00**	**0.01**	**0.08**	**0.01**	**0.03**	**0.00**
Mar	02 March 2022	130	39	30	Postfrontal, high pressure	0.27	0.08	0.00	0.01	0.17	0.00	0.02	0.00
	03 March 2022	131, 132	71	53	Weak prefrontal	0.74	0.12	0.00	0.03	0.26	0.03	0.04	0.00
	04 March 2022	133, 134	42	29	Cold high pressure	1.64	0.02	0.00	0.06	0.05	0.06	0.01	0.00
	13 March 2022	138	8	2	Postfrontal, CAO conditions	0.00	0.11	0.00	0.00	0.59	0.00	0.08	0.00
	14 March 2022	139, 140	38	32	Late postfrontal, cold high pressure; smoke plume sampled from a woodland fire	0.08	0.03	0.00	0.00	0.05	0.00	0.04	0.01
	18 March 2022	141	14	12	Weak postfrontal	0.12	0.02	0.00	0.00	0.03	0.00	0.03	0.07
	26 March 2022	144, 145	29	15	Postfrontal; sampled dust, smoke, and potentially pollen	0.02	0.02	0.00	0.00	0.05	0.00	0.04	0.01
	28 March 2022	146	17	10	Postfrontal	0.02	0.03	0.00	0.00	0.05	0.00	0.05	0.00

	29 March 2022	147, 148	19	4	Postfrontal, high pressure, CAO conditions	0.09	0.08	0.00	0.00	0.16	0.00	0.05	0.02
	Overall		**277**	**187**		**0.22**	**0.05**	**0.00**	**0.01**	**0.12**	**0.01**	**0.03**	**0.00**
May	03 May 2022	149	15	10	Weak prefrontal; presence of smoke potentially from New Mexico	0.37	0.08	0.00	0.01	0.14	0.01	0.05	0.00
	05 May 2022	150, 151	18	9	Postfrontal	0.03	0.02	0.00	0.00	0.04	0.00	0.02	0.00
	16 May 2022	153, 154	39	5	Prefrontal to an approaching cold front yet also postfrontal to a departing band of precipitation	0.12	0.16	0.00	0.00	0.31	0.00	0.03	0.00
	17 May 2022	155	37	2	Postfrontal	0.06	0.00	0.00	0.00	0.01	0.00	0.01	0.00
	20 May 2022	158	28	19	Warm high pressure, southerly flow due to Bermuda high[2]; haze with potential sampling of bioaerosol	2.19	0.01	0.00	0.08	0.06	0.05	0.00	0.00
	Overall		**137**	**45**		**0.39**	**0.02**	**0.00**	**0.01**	**0.08**	**0.01**	**0.01**	**0.00**
Mar transit	22 March 2022	142, 143	48	47	High pressure, two days after a cold front and two days before another cold front	0.74	0.04	0.00	0.03	0.10	0.01	0.06	0.00
May transit	18 May 2022	156, 157	67	23	Postfrontal along East Coast, aircraft passed across the cold front on the way to Bermuda	1.10	0.00	0.00	0.04	0.01	0.02	0.00	0.00
	21 May 2022	159, 160	42	14	Warm high pressure, anticyclonic flow around Bermuda high	1.14	0.00	0.00	0.04	0.01	0.03	0.00	0.00
	31 May 2022	161	11	1	Postfrontal	0.18	0.01	0.01	0.01	0.02	0.01	0.02	0.20
	Overall		**120**	**38**		**1.07**	**0.00**	**0.00**	**0.04**	**0.01**	**0.02**	**0.00**	**0.00**
Jun Bermuda	02 June 2022	162, 163	4	1	Prefrontal	0.83	0.00	0.00	0.03	0.00	0.03	0.00	0.13
	03 June 2022	164	1	0	Prefrontal, tropical system approaching from the southwest	NaN	NaN	NaN	NaN	NaN	NaN	NaN	NaN
	05 June 2022	165	29	24	Could only fly in the morning due to approaching tropical cyclone	1.97	0.00	0.00	0.07	0.00	0.06	0.00	0.00

					(TC), TC departs 06 June 2022.								
	07 June 2022	167	1	0	High behind departing TC	NaN	NaN	NaN	NaN	NaN	NaN	NaN	NaN
	08 June 2022	168, 169	2	1	High pressure behind TC, African dust known to be in domain	5.56	0.47	0.09	0.21	0.86	0.20	0.86	1.97
	10 June 2022	170	1	1	High pressure, isolated thunderstorms, African dust known to be in domain	2.28	0.00	0.00	0.06	0.00	0.01	0.00	0.00
	11 June 2022	172, 173	20	7	High pressure, African dust known to be in domain	0.78	0.10	0.00	0.03	0.20	0.02	0.02	0.00
	13 June 2022	174	25	17	High pressure, African dust known to be in domain but sampled away from dust for contrast	1.31	0.00	0.00	0.05	0.00	0.04	0.00	0.00
	Overall		**83**	**51**		**1.38**	**0.00**	**0.00**	**0.05**	**0.01**	**0.04**	**0.00**	**0.00**

[1]Davis et al. (1997)

Table S9. Same as Table S8, except forest fire burning of pinion and juniper trees is considered as the only combustion process contributing to Na^{+}_{comb} and K^{+}_{comb}.

Category	Date	RF(s)	N PILS samples	N samples w/ derived species	Meteorological conditions and/or relevant notes	Median $ssNa^{+}$ ($\mu g\ m^{-3}$)	Median Na^{+}_{dust} ($\mu g\ m^{-3}$)	Median Na^{+}_{comb} ($\mu g\ m^{-3}$)	Median $ssCa^{2+}$ ($\mu g\ m^{-3}$)	Median Ca^{2+}_{dust} ($\mu g\ m^{-3}$)	Median ssK^{+} ($\mu g\ m^{-3}$)	Median K^{+}_{dust} ($\mu g\ m^{-3}$)	Median K^{+}_{comb} ($\mu g\ m^{-3}$)
Dec-Feb	30 November 2021	94	7	1	Remains of post-frontal conditions	0.00	0.16	0.00	0.00	0.41	0.00	0.06	0.00
	01 December 2021	95	16	14	Prefrontal, high pressure; smoke in boundary layer near coast	0.11	0.21	0.00	0.00	0.48	0.00	0.05	0.00
	07 December 2021	96	5	3	Postfrontal, cold high pressure behind a strong cold front	0.09	0.10	0.00	0.00	0.22	0.00	0.03	0.00
	11 January 2022	100, 101	6	3	Cold high pressure, cold air outbreak (CAO) conditions	0.34	0.03	0.00	0.01	0.08	0.01	0.01	0.00
	12 January 2022	102, 103	33	11	Cold high pressure	0.16	0.04	0.00	0.01	0.08	0.00	0.02	0.00
	15 January 2022	104	3	2	Postfrontal	0.67	0.02	0.00	0.01	0.04	0.01	0.00	0.00
	18 January 2022	105	11	0	Low pressure moves offshore, sets up CAO conditions	NaN	NaN	NaN	NaN	NaN	NaN	NaN	NaN
	19 January 2022	107, 108	26	6	Short-lived high pressure	0.27	0.04	0.01	0.01	0.07	0.01	0.05	0.06
	24 January 2022	109, 110	26	9	Postfrontal, weak high pressure	0.19	0.04	0.00	0.00	0.07	0.01	0.05	0.02
	26 January 2022	111, 112	20	7	Postfrontal	0.32	0.02	0.04	0.01	0.04	0.01	0.03	0.35
	27 January 2022	113, 114	18	4	Cold high pressure	0.28	0.00	0.00	0.01	0.00	0.01	0.00	0.00
	01 February 2022	115	8	4	High pressure	1.09	0.01	0.00	0.02	0.03	0.02	0.00	0.00
	02 February 2022	116	17	4	High pressure	0.74	0.00	0.00	0.02	0.01	0.03	0.00	0.02

	03 February 2022	117, 118	15	4	High pressure	1.16	0.00	0.00	0.03	0.00	0.04	0.00	0.01
	15 February 2022	120, 121	34	7	Postfrontal conditions, cold high pressure	0.15	0.04	0.00	0.01	0.13	0.01	0.02	0.00
	16 February 2022	122, 123	21	10	Cold high pressure	0.14	0.05	0.00	0.01	0.12	0.00	0.04	0.00
	19 February 2022	124, 125	38	18	Weak postfrontal	0.06	0.02	0.00	0.00	0.11	0.00	0.04	0.00
	22 February 2022	126, 127	25	20	Prefrontal, high pressure	1.69	0.03	0.00	0.04	0.07	0.04	0.00	0.00
	26 February 2022	128, 129	16	14	Postfrontal	0.10	0.02	0.00	0.00	0.05	0.00	0.04	0.00
	Overall		**345**	**141**		**0.21**	**0.03**	**0.00**	**0.01**	**0.08**	**0.01**	**0.03**	**0.00**
Mar	02 March 2022	130	39	30	Postfrontal, high pressure	0.27	0.07	0.00	0.01	0.17	0.00	0.02	0.00
	03 March 2022	131, 132	71	53	Weak prefrontal	0.76	0.11	0.00	0.03	0.26	0.03	0.04	0.00
	04 March 2022	133, 134	42	29	Cold high pressure	1.65	0.01	0.00	0.06	0.05	0.06	0.01	0.00
	13 March 2022	138	8	2	Postfrontal, CAO conditions	0.00	0.11	0.00	0.00	0.59	0.00	0.08	0.00
	14 March 2022	139, 140	38	32	Late postfrontal, cold high pressure; smoke plume sampled from a woodland fire	0.08	0.03	0.00	0.00	0.05	0.00	0.04	0.01
	18 March 2022	141	14	12	Weak postfrontal	0.12	0.02	0.01	0.00	0.03	0.00	0.03	0.07
	26 March 2022	144, 145	29	15	Postfrontal; sampled dust, smoke, and potentially pollen	0.02	0.02	0.00	0.00	0.05	0.00	0.04	0.01
	28 March 2022	146	17	10	Postfrontal	0.01	0.03	0.00	0.00	0.05	0.00	0.05	0.00
	29 March 2022	147, 148	19	4	Postfrontal, high pressure, CAO conditions	0.09	0.08	0.00	0.00	0.16	0.00	0.05	0.02
	Overall		**277**	**187**		**0.23**	**0.05**	**0.00**	**0.01**	**0.12**	**0.01**	**0.03**	**0.00**
May	03 May 2022	149	15	10	Weak prefrontal; presence of smoke potentially from New Mexico	0.38	0.07	0.00	0.01	0.14	0.01	0.05	0.00

	05 May 2022	150, 151	18	9	Postfrontal	0.03	0.02	0.00	0.00	0.04	0.00	0.02	0.00
	16 May 2022	153, 154	39	5	Prefrontal to an approaching cold front yet also postfrontal to a departing band of precipitation	0.13	0.15	0.00	0.00	0.31	0.00	0.03	0.00
	17 May 2022	155	37	2	Postfrontal	0.06	0.00	0.00	0.00	0.01	0.00	0.01	0.00
	20 May 2022	158	28	19	Warm high pressure, southerly flow due to Bermuda high[2]; haze with potential sampling of bioaerosol	2.21	0.00	0.00	0.08	0.06	0.06	0.00	0.00
	Overall		**137**	**45**		**0.41**	**0.02**	**0.00**	**0.01**	**0.08**	**0.01**	**0.01**	**0.00**
Mar transit	22 March 2022	142, 143	48	47	High pressure, two days after a cold front and two days before another cold front	0.75	0.04	0.00	0.03	0.10	0.01	0.06	0.00
May transit	18 May 2022	156, 157	67	23	Postfrontal along East Coast, aircraft passed across the cold front on the way to Bermuda	1.11	0.00	0.00	0.04	0.01	0.02	0.00	0.00
	21 May 2022	159, 160	42	14	Warm high pressure, anticyclonic flow around Bermuda high	1.14	0.00	0.00	0.04	0.01	0.03	0.00	0.00
	31 May 2022	161	11	1	Postfrontal	0.17	0.01	0.02	0.01	0.02	0.01	0.02	0.20
	Overall		**120**	**38**		**1.08**	**0.00**	**0.00**	**0.04**	**0.01**	**0.02**	**0.00**	**0.00**
Jun Bermuda	02 June 2022	162, 163	4	1	Prefrontal	0.82	0.00	0.01	0.03	0.00	0.03	0.00	0.13
	03 June 2022	164	1	0	Prefrontal, tropical system approaching from the southwest	NaN	NaN	NaN	NaN	NaN	NaN	NaN	NaN
	05 June 2022	165	29	24	Could only fly in the morning due to approaching tropical cyclone (TC), TC departs 06 June 2022.	1.97	0.00	0.00	0.07	0.00	0.06	0.00	0.00
	07 June 2022	167	1	0	High behind departing TC	NaN	NaN	NaN	NaN	NaN	NaN	NaN	NaN
	08 June 2022	168, 169	2	1	High pressure behind TC, African dust known to be in domain	5.47	0.45	0.20	0.21	0.87	0.20	0.87	1.97

	10 June 2022	170	1	1	High pressure, isolated thunderstorms, African dust known to be in domain	2.28	0.00	0.00	0.06	0.00	0.01	0.00	0.00
	11 June 2022	172, 173	20	7	High pressure, African dust known to be in domain	0.80	0.09	0.00	0.03	0.20	0.02	0.01	0.00
	13 June 2022	174	25	17	High pressure, African dust known to be in domain but sampled away from dust for contrast	1.32	0.00	0.00	0.05	0.00	0.04	0.00	0.00
	Overall		**83**	**51**		**1.38**	**0.00**	**0.00**	**0.05**	**0.01**	**0.04**	**0.00**	**0.00**

[1]Davis et al. (1997)

Table S10. Same as Table S8, except industrial operations (i.e., those at steel mills and cement plants) are considered as the only combustion process contributing to Na^+_{comb} and K^+_{comb}.

Category	Date	RF(s)	N PILS samples	N samples w/ derived species	Meteorological conditions and/or relevant notes	Median $ssNa^+$ ($\mu g\ m^{-3}$)	Median Na^+_{dust} ($\mu g\ m^{-3}$)	Median Na^+_{comb} ($\mu g\ m^{-3}$)	Median $ssCa^{2+}$ ($\mu g\ m^{-3}$)	Median Ca^{2+}_{dust} ($\mu g\ m^{-3}$)	Median ssK^+ ($\mu g\ m^{-3}$)	Median K^+_{dust} ($\mu g\ m^{-3}$)	Median K^+_{comb} ($\mu g\ m^{-3}$)
Dec-Feb	30 November 2021	94	7	1	Remains of post-frontal conditions	0.01	0.14	0.00	0.00	0.41	0.00	0.06	0.00
	01 December 2021	95	16	14	Prefrontal, high pressure; smoke in boundary layer near coast	0.18	0.16	0.00	0.01	0.48	0.01	0.05	0.00
	07 December 2021	96	5	3	Postfrontal, cold high pressure behind a strong cold front	0.12	0.07	0.00	0.00	0.22	0.00	0.02	0.00
	11 January 2022	100, 101	6	3	Cold high pressure, cold air outbreak (CAO) conditions	0.35	0.03	0.00	0.01	0.08	0.01	0.01	0.00
	12 January 2022	102, 103	33	11	Cold high pressure	0.16	0.03	0.00	0.01	0.08	0.00	0.02	0.00
	15 January 2022	104	3	2	Postfrontal	0.68	0.01	0.00	0.01	0.04	0.01	0.00	0.00
	18 January 2022	105	11	0	Low pressure moves offshore, sets up CAO conditions	NaN	NaN	NaN	NaN	NaN	NaN	NaN	NaN
	19 January 2022	107, 108	26	6	Short-lived high pressure	0.26	0.03	0.02	0.01	0.07	0.01	0.05	0.06
	24 January 2022	109, 110	26	9	Postfrontal, weak high pressure	0.22	0.04	0.00	0.00	0.08	0.01	0.05	0.02
	26 January 2022	111, 112	20	7	Postfrontal	0.27	0.01	0.09	0.01	0.04	0.01	0.04	0.35
	27 January 2022	113, 114	18	4	Cold high pressure	0.28	0.00	0.00	0.01	0.00	0.01	0.00	0.00
	01 February 2022	115	8	4	High pressure	1.10	0.00	0.00	0.02	0.03	0.02	0.00	0.00
	02 February 2022	116	17	4	High pressure	0.75	0.00	0.00	0.02	0.01	0.03	0.00	0.02

	03 February 2022	117, 118	15	4	High pressure	1.16	0.00	0.00	0.03	0.00	0.04	0.00	0.01
	15 February 2022	120, 121	34	7	Postfrontal conditions, cold high pressure	0.23	0.04	0.00	0.01	0.13	0.01	0.01	0.00
	16 February 2022	122, 123	21	10	Cold high pressure	0.15	0.04	0.00	0.01	0.12	0.00	0.04	0.00
	19 February 2022	124, 125	38	18	Weak postfrontal	0.06	0.02	0.00	0.00	0.11	0.00	0.04	0.00
	22 February 2022	126, 127	25	20	Prefrontal, high pressure	1.73	0.00	0.00	0.05	0.07	0.04	0.00	0.00
	26 February 2022	128, 129	16	14	Postfrontal	0.09	0.02	0.00	0.00	0.05	0.00	0.04	0.00
	Overall		**345**	**141**		**0.23**	**0.02**	**0.00**	**0.01**	**0.08**	**0.01**	**0.03**	**0.00**
Mar	02 March 2022	130	39	30	Postfrontal, high pressure	0.29	0.04	0.00	0.01	0.17	0.00	0.02	0.00
	03 March 2022	131, 132	71	53	Weak prefrontal	0.81	0.07	0.00	0.03	0.26	0.03	0.04	0.00
	04 March 2022	133, 134	42	29	Cold high pressure	1.66	0.00	0.00	0.06	0.05	0.06	0.01	0.00
	13 March 2022	138	8	2	Postfrontal, CAO conditions	0.00	0.11	0.00	0.00	0.59	0.00	0.08	0.00
	14 March 2022	139, 140	38	32	Late postfrontal, cold high pressure; smoke plume sampled from a woodland fire	0.09	0.03	0.00	0.00	0.05	0.00	0.04	0.01
	18 March 2022	141	14	12	Weak postfrontal	0.11	0.02	0.02	0.00	0.03	0.00	0.03	0.07
	26 March 2022	144, 145	29	15	Postfrontal; sampled dust, smoke, and potentially pollen	0.02	0.02	0.00	0.00	0.05	0.00	0.04	0.01
	28 March 2022	146	17	10	Postfrontal	0.01	0.03	0.00	0.00	0.05	0.00	0.05	0.00
	29 March 2022	147, 148	19	4	Postfrontal, high pressure, CAO conditions	0.10	0.07	0.01	0.00	0.16	0.00	0.05	0.02
	Overall		**277**	**187**		**0.22**	**0.03**	**0.00**	**0.01**	**0.12**	**0.01**	**0.03**	**0.00**
May	03 May 2022	149	15	10	Weak prefrontal; presence of smoke potentially from New Mexico	0.41	0.06	0.00	0.01	0.14	0.01	0.05	0.00

	05 May 2022	150, 151	18	9	Postfrontal	0.03	0.02	0.00	0.00	0.04	0.00	0.03	0.00
	16 May 2022	153, 154	39	5	Prefrontal to an approaching cold front yet also postfrontal to a departing band of precipitation	0.16	0.10	0.00	0.01	0.31	0.01	0.03	0.00
	17 May 2022	155	37	2	Postfrontal	0.06	0.00	0.00	0.00	0.01	0.00	0.01	0.00
	20 May 2022	158	28	19	Warm high pressure, southerly flow due to Bermuda high[2]; haze with potential sampling of bioaerosol	2.24	0.00	0.00	0.08	0.06	0.06	0.00	0.00
	Overall		**137**	**45**		**0.45**	**0.01**	**0.00**	**0.01**	**0.08**	**0.01**	**0.01**	**0.00**
Mar transit	22 March 2022	142, 143	48	47	High pressure, two days after a cold front and two days before another cold front	0.77	0.02	0.00	0.03	0.10	0.01	0.06	0.00
May transit	18 May 2022	156, 157	67	23	Postfrontal along East Coast, aircraft passed across the cold front on the way to Bermuda	1.11	0.00	0.00	0.04	0.01	0.02	0.00	0.00
	21 May 2022	159, 160	42	14	Warm high pressure, anticyclonic flow around Bermuda high	1.14	0.00	0.00	0.04	0.01	0.03	0.00	0.00
	31 May 2022	161	11	1	Postfrontal	0.14	0.01	0.05	0.01	0.02	0.01	0.02	0.20
	Overall		**120**	**38**		**1.08**	**0.00**	**0.00**	**0.04**	**0.01**	**0.02**	**0.00**	**0.00**
Jun Bermuda	02 June 2022	162, 163	4	1	Prefrontal	0.81	0.00	0.02	0.03	0.00	0.03	0.00	0.13
	03 June 2022	164	1	0	Prefrontal, tropical system approaching from the southwest	NaN	NaN	NaN	NaN	NaN	NaN	NaN	NaN
	05 June 2022	165	29	24	Could only fly in the morning due to approaching tropical cyclone (TC), TC departs 06 June 2022.	1.97	0.00	0.00	0.07	0.00	0.06	0.00	0.00
	07 June 2022	167	1	0	High behind departing TC	NaN	NaN	NaN	NaN	NaN	NaN	NaN	NaN
	08 June 2022	168, 169	2	1	High pressure behind TC, African dust known to be in domain	5.24	0.39	0.48	0.20	0.88	0.19	0.88	1.97

	10 June 2022	170	1	1	High pressure, isolated thunderstorms, African dust known to be in domain	2.28	0.00	0.00	0.06	0.00	0.01	0.00	0.00
	11 June 2022	172, 173	20	7	High pressure, African dust known to be in domain	0.83	0.06	0.00	0.03	0.20	0.02	0.01	0.00
	13 June 2022	174	25	17	High pressure, African dust known to be in domain but sampled away from dust for contrast	1.35	0.00	0.00	0.05	0.00	0.04	0.00	0.00
	Overall		**83**	**51**		**1.38**	**0.00**	**0.00**	**0.05**	**0.01**	**0.04**	**0.00**	**0.00**

[1]Davis et al. (1997)

Table S11. Same as Table S8, except inefficient batch combustion in a sauna stove is considered as the only combustion process contributing to Na^{+}_{comb} and K^{+}_{comb}.

Category	Date	RF(s)	N PILS samples	N samples w/ derived species	Meteorological conditions and/or relevant notes	Median $ssNa^{+}$ ($\mu g\ m^{-3}$)	Median Na^{+}_{dust} ($\mu g\ m^{-3}$)	Median Na^{+}_{comb} ($\mu g\ m^{-3}$)	Median $ssCa^{2+}$ ($\mu g\ m^{-3}$)	Median Ca^{2+}_{dust} ($\mu g\ m^{-3}$)	Median ssK^{+} ($\mu g\ m^{-3}$)	Median K^{+}_{dust} ($\mu g\ m^{-3}$)	Median K^{+}_{comb} ($\mu g\ m^{-3}$)
Dec-Feb	30 November 2021	94	7	1	Remains of post-frontal conditions	0.16	0.00	0.00	0.01	0.40	0.01	0.06	0.00
	01 December 2021	95	16	14	Prefrontal, high pressure; smoke in boundary layer near coast	0.35	0.00	0.00	0.01	0.47	0.01	0.05	0.00
	07 December 2021	96	5	3	Postfrontal, cold high pressure behind a strong cold front	0.19	0.00	0.00	0.01	0.22	0.01	0.02	0.00
	11 January 2022	100, 101	6	3	Cold high pressure, cold air outbreak (CAO) conditions	0.36	0.00	0.00	0.01	0.08	0.01	0.01	0.00
	12 January 2022	102, 103	33	11	Cold high pressure	0.21	0.00	0.00	0.01	0.08	0.00	0.02	0.00
	15 January 2022	104	3	2	Postfrontal	0.69	0.00	0.00	0.01	0.04	0.01	0.00	0.00
	18 January 2022	105	11	0	Low pressure moves offshore, sets up CAO conditions	NaN	NaN	NaN	NaN	NaN	NaN	NaN	NaN
	19 January 2022	107, 108	26	6	Short-lived high pressure	0.22	0.02	0.05	0.01	0.07	0.01	0.06	0.06
	24 January 2022	109, 110	26	9	Postfrontal, weak high pressure	0.07	0.00	0.01	0.00	0.09	0.00	0.05	0.02
	26 January 2022	111, 112	20	7	Postfrontal	0.12	0.00	0.27	0.00	0.04	0.00	0.04	0.35
	27 January 2022	113, 114	18	4	Cold high pressure	0.28	0.00	0.00	0.01	0.00	0.01	0.00	0.00
	01 February 2022	115	8	4	High pressure	1.10	0.00	0.00	0.02	0.03	0.02	0.00	0.00
	02 February 2022	116	17	4	High pressure	0.74	0.00	0.00	0.02	0.01	0.03	0.00	0.02

	03 February 2022	117, 118	15	4	High pressure	1.16	0.00	0.00	0.03	0.00	0.04	0.00	0.01
	15 February 2022	120, 121	34	7	Postfrontal conditions, cold high pressure	0.31	0.00	0.00	0.01	0.13	0.01	0.01	0.00
	16 February 2022	122, 123	21	10	Cold high pressure	0.23	0.00	0.00	0.01	0.12	0.01	0.03	0.00
	19 February 2022	124, 125	38	18	Weak postfrontal	0.08	0.01	0.00	0.00	0.11	0.00	0.04	0.00
	22 February 2022	126, 127	25	20	Prefrontal, high pressure	1.73	0.00	0.00	0.05	0.07	0.04	0.00	0.00
	26 February 2022	128, 129	16	14	Postfrontal	0.10	0.01	0.00	0.00	0.05	0.00	0.04	0.00
	Overall		**345**	**141**		**0.24**	**0.00**	**0.00**	**0.01**	**0.08**	**0.01**	**0.02**	**0.00**
	02 March 2022	130	39	30	Postfrontal, high pressure	0.31	0.00	0.00	0.01	0.17	0.01	0.01	0.00
	03 March 2022	131, 132	71	53	Weak prefrontal	0.86	0.00	0.00	0.03	0.26	0.03	0.03	0.00
	04 March 2022	133, 134	42	29	Cold high pressure	1.51	0.00	0.00	0.05	0.05	0.05	0.01	0.00
	13 March 2022	138	8	2	Postfrontal, CAO conditions	0.11	0.00	0.00	0.00	0.59	0.00	0.08	0.00
	14 March 2022	139, 140	38	32	Late postfrontal, cold high pressure; smoke plume sampled from a woodland fire	0.08	0.01	0.01	0.00	0.06	0.00	0.04	0.01
Mar	18 March 2022	141	14	12	Weak postfrontal	0.10	0.01	0.05	0.00	0.04	0.00	0.04	0.07
	26 March 2022	144, 145	29	15	Postfrontal; sampled dust, smoke, and potentially pollen	0.03	0.02	0.01	0.00	0.05	0.00	0.04	0.01
	28 March 2022	146	17	10	Postfrontal	0.05	0.00	0.00	0.00	0.05	0.00	0.04	0.00
	29 March 2022	147, 148	19	4	Postfrontal, high pressure, CAO conditions	0.12	0.03	0.02	0.00	0.15	0.00	0.05	0.02
	Overall		**277**	**187**		**0.25**	**0.00**	**0.00**	**0.01**	**0.12**	**0.01**	**0.03**	**0.00**
May	03 May 2022	149	15	10	Weak prefrontal; presence of smoke potentially from New Mexico	0.43	0.00	0.00	0.01	0.14	0.02	0.05	0.00

	05 May 2022	150, 151	18	9	Postfrontal	0.02	0.00	0.00	0.00	0.05	0.00	0.03	0.00
	16 May 2022	153, 154	39	5	Prefrontal to an approaching cold front yet also postfrontal to a departing band of precipitation	0.26	0.00	0.00	0.01	0.31	0.01	0.02	0.00
	17 May 2022	155	37	2	Postfrontal	0.06	0.00	0.00	0.00	0.01	0.00	0.01	0.00
	20 May 2022	158	28	19	Warm high pressure, southerly flow due to Bermuda high[2]; haze with potential sampling of bioaerosol	2.24	0.00	0.00	0.08	0.06	0.06	0.00	0.00
	Overall		**137**	**45**		**0.45**	**0.00**	**0.00**	**0.02**	**0.08**	**0.01**	**0.01**	**0.00**
Mar transit	22 March 2022	142, 143	48	47	High pressure, two days after a cold front and two days before another cold front	0.72	0.00	0.00	0.03	0.10	0.02	0.05	0.00
	18 May 2022	156, 157	67	23	Postfrontal along East Coast, aircraft passed across the cold front on the way to Bermuda	1.11	0.00	0.00	0.04	0.01	0.02	0.00	0.00
May transit	21 May 2022	159, 160	42	14	Warm high pressure, anticyclonic flow around Bermuda high	1.14	0.00	0.00	0.04	0.01	0.03	0.00	0.00
	31 May 2022	161	11	1	Postfrontal	0.04	0.01	0.15	0.00	0.02	0.00	0.02	0.20
	Overall		**120**	**38**		**1.08**	**0.00**	**0.00**	**0.04**	**0.01**	**0.02**	**0.00**	**0.00**
	02 June 2022	162, 163	4	1	Prefrontal	0.77	0.00	0.05	0.03	0.00	0.03	0.00	0.13
	03 June 2022	164	1	0	Prefrontal, tropical system approaching from the southwest	NaN	NaN	NaN	NaN	NaN	NaN	NaN	NaN
Jun Bermuda	05 June 2022	165	29	24	Could only fly in the morning due to approaching tropical cyclone (TC), TC departs 06 June 2022.	1.97	0.00	0.00	0.07	0.00	0.06	0.00	0.00
	07 June 2022	167	1	0	High behind departing TC	NaN	NaN	NaN	NaN	NaN	NaN	NaN	NaN
	08 June 2022	168, 169	2	1	High pressure behind TC, African dust known to be in domain	4.37	0.26	1.48	0.17	0.91	0.16	0.91	1.97

	10 June 2022	170	1	1	High pressure, isolated thunderstorms, African dust known to be in domain	2.28	0.00	0.00	0.06	0.00	0.01	0.00	0.00
	11 June 2022	172, 173	20	7	High pressure, African dust known to be in domain	0.89	0.00	0.00	0.03	0.19	0.03	0.01	0.00
	13 June 2022	174	25	17	High pressure, African dust known to be in domain but sampled away from dust for contrast	1.38	0.00	0.00	0.05	0.00	0.04	0.00	0.00
	Overall		**83**	**51**		**1.42**	**0.00**	**0.00**	**0.05**	**0.01**	**0.04**	**0.00**	**0.00**

[1]Davis et al. (1997)

Table S12. Same as Table S8, except fossil fuel combustion by motor vehicles is considered as the only combustion process contributing to Na^{+}_{comb} and K^{+}_{comb}.

Category	Date	RF(s)	N PILS samples	N samples w/ derived species	Meteorological conditions and/or relevant notes	Median $ssNa^{+}$ ($\mu g\ m^{-3}$)	Median Na^{+}_{dust} ($\mu g\ m^{-3}$)	Median Na^{+}_{comb} ($\mu g\ m^{-3}$)	Median $ssCa^{2+}$ ($\mu g\ m^{-3}$)	Median Ca^{2+}_{dust} ($\mu g\ m^{-3}$)	Median ssK^{+} ($\mu g\ m^{-3}$)	Median K^{+}_{dust} ($\mu g\ m^{-3}$)	Median K^{+}_{comb} ($\mu g\ m^{-3}$)
Dec-Feb	30 November 2021	94	7	1	Remains of post-frontal conditions	0.16	0.00	0.00	0.01	0.40	0.01	0.06	0.00
	01 December 2021	95	16	14	Prefrontal, high pressure; smoke in boundary layer near coast	0.35	0.00	0.00	0.01	0.47	0.01	0.05	0.00
	07 December 2021	96	5	3	Postfrontal, cold high pressure behind a strong cold front	0.19	0.00	0.00	0.01	0.22	0.01	0.02	0.00
	11 January 2022	100, 101	6	3	Cold high pressure, cold air outbreak (CAO) conditions	0.36	0.00	0.00	0.01	0.08	0.01	0.01	0.00
	12 January 2022	102, 103	33	11	Cold high pressure	0.21	0.00	0.00	0.01	0.08	0.00	0.02	0.00
	15 January 2022	104	3	2	Postfrontal	0.69	0.00	0.00	0.01	0.04	0.01	0.00	0.00
	18 January 2022	105	11	0	Low pressure moves offshore, sets up CAO conditions	NaN	NaN	NaN	NaN	NaN	NaN	NaN	NaN
	19 January 2022	107, 108	26	6	Short-lived high pressure	0.21	0.01	0.05	0.01	0.07	0.01	0.06	0.06
	24 January 2022	109, 110	26	9	Postfrontal, weak high pressure	0.07	0.00	0.02	0.00	0.09	0.00	0.05	0.02
	26 January 2022	111, 112	20	7	Postfrontal	0.05	0.00	0.32	0.00	0.05	0.00	0.05	0.35
	27 January 2022	113, 114	18	4	Cold high pressure	0.28	0.00	0.00	0.01	0.00	0.01	0.00	0.00
	01 February 2022	115	8	4	High pressure	1.10	0.00	0.00	0.02	0.03	0.02	0.00	0.00
	02 February 2022	116	17	4	High pressure	0.74	0.00	0.00	0.02	0.01	0.03	0.00	0.02

	03 February 2022	117, 118	15	4	High pressure	1.16	0.00	0.00	0.03	0.00	0.04	0.00	0.01
	15 February 2022	120, 121	34	7	Postfrontal conditions, cold high pressure	0.31	0.00	0.00	0.01	0.13	0.01	0.01	0.00
	16 February 2022	122, 123	21	10	Cold high pressure	0.22	0.00	0.00	0.01	0.12	0.01	0.03	0.00
	19 February 2022	124, 125	38	18	Weak postfrontal	0.07	0.00	0.00	0.00	0.11	0.00	0.04	0.00
	22 February 2022	126, 127	25	20	Prefrontal, high pressure	1.73	0.00	0.00	0.05	0.07	0.04	0.00	0.00
	26 February 2022	128, 129	16	14	Postfrontal	0.10	0.00	0.00	0.00	0.05	0.00	0.04	0.00
	Overall		**345**	**141**		**0.24**	**0.00**	**0.00**	**0.01**	**0.08**	**0.01**	**0.02**	**0.00**
	02 March 2022	130	39	30	Postfrontal, high pressure	0.29	0.00	0.00	0.01	0.17	0.01	0.01	0.00
	03 March 2022	131, 132	71	53	Weak prefrontal	0.86	0.00	0.00	0.03	0.26	0.03	0.03	0.00
	04 March 2022	133, 134	42	29	Cold high pressure	1.51	0.00	0.00	0.05	0.05	0.05	0.01	0.00
	13 March 2022	138	8	2	Postfrontal, CAO conditions	0.11	0.00	0.00	0.00	0.59	0.00	0.08	0.00
	14 March 2022	139, 140	38	32	Late postfrontal, cold high pressure; smoke plume sampled from a woodland fire	0.08	0.00	0.01	0.00	0.06	0.00	0.04	0.01
Mar	18 March 2022	141	14	12	Weak postfrontal	0.08	0.01	0.06	0.00	0.04	0.00	0.04	0.07
	26 March 2022	144, 145	29	15	Postfrontal; sampled dust, smoke, and potentially pollen	0.04	0.02	0.01	0.00	0.05	0.00	0.04	0.01
	28 March 2022	146	17	10	Postfrontal	0.05	0.00	0.00	0.00	0.05	0.00	0.04	0.00
	29 March 2022	147, 148	19	4	Postfrontal, high pressure, CAO conditions	0.13	0.02	0.02	0.00	0.15	0.00	0.05	0.02
	Overall		**277**	**187**		**0.25**	**0.00**	**0.00**	**0.01**	**0.12**	**0.01**	**0.03**	**0.00**
May	03 May 2022	149	15	10	Weak prefrontal; presence of smoke potentially from New Mexico	0.40	0.00	0.00	0.01	0.14	0.01	0.05	0.00

	05 May 2022	150, 151	18	9	Postfrontal	0.02	0.00	0.00	0.00	0.05	0.00	0.03	0.00
	16 May 2022	153, 154	39	5	Prefrontal to an approaching cold front yet also postfrontal to a departing band of precipitation	0.29	0.00	0.00	0.01	0.31	0.01	0.02	0.00
	17 May 2022	155	37	2	Postfrontal	0.06	0.00	0.00	0.00	0.01	0.00	0.01	0.00
	20 May 2022	158	28	19	Warm high pressure, southerly flow due to Bermuda high[2]; haze with potential sampling of bioaerosol	2.24	0.00	0.00	0.08	0.06	0.06	0.00	0.00
	Overall		**137**	**45**		**0.42**	**0.00**	**0.00**	**0.01**	**0.08**	**0.01**	**0.01**	**0.00**
Mar transit	22 March 2022	142, 143	48	47	High pressure, two days after a cold front and two days before another cold front	0.72	0.00	0.00	0.03	0.10	0.02	0.05	0.00
	18 May 2022	156, 157	67	23	Postfrontal along East Coast, aircraft passed across the cold front on the way to Bermuda	1.11	0.00	0.00	0.04	0.01	0.02	0.00	0.00
May transit	21 May 2022	159, 160	42	14	Warm high pressure, anticyclonic flow around Bermuda high	1.14	0.00	0.00	0.04	0.01	0.03	0.00	0.00
	31 May 2022	161	11	1	Postfrontal	0.01	0.01	0.18	0.00	0.02	0.00	0.02	0.20
	Overall		**120**	**38**		**1.08**	**0.00**	**0.00**	**0.04**	**0.01**	**0.02**	**0.00**	**0.00**
	02 June 2022	162, 163	4	1	Prefrontal	0.76	0.00	0.07	0.03	0.00	0.03	0.00	0.13
	03 June 2022	164	1	0	Prefrontal, tropical system approaching from the southwest	NaN	NaN	NaN	NaN	NaN	NaN	NaN	NaN
Jun Bermuda	05 June 2022	165	29	24	Could only fly in the morning due to approaching tropical cyclone (TC), TC departs 06 June 2022.	1.97	0.00	0.00	0.07	0.00	0.06	0.00	0.00
	07 June 2022	167	1	0	High behind departing TC	NaN	NaN	NaN	NaN	NaN	NaN	NaN	NaN
	08 June 2022	168, 169	2	1	High pressure behind TC, African dust known to be in domain	4.09	0.23	1.79	0.16	0.92	0.15	0.92	1.97

	10 June 2022	170	1	1	High pressure, isolated thunderstorms, African dust known to be in domain	2.28	0.00	0.00	0.06	0.00	0.01	0.00	0.00
	11 June 2022	172, 173	20	7	High pressure, African dust known to be in domain	0.89	0.00	0.00	0.03	0.19	0.03	0.01	0.00
	13 June 2022	174	25	17	High pressure, African dust known to be in domain but sampled away from dust for contrast	1.38	0.00	0.00	0.05	0.00	0.04	0.00	0.00
	Overall		**83**	**51**		**1.42**	**0.00**	**0.00**	**0.05**	**0.01**	**0.04**	**0.00**	**0.00**

[1]Davis et al. (1997)

Table S13. Same as Table S8, except burning of pulverized western coal comprised of low sulfur (0.5%) and high ash (22%) at a coal-fired power plant is considered as the only combustion process contributing to Na^+_{comb} and K^+_{comb}.

Category	Date	RF(s)	N PILS samples	N samples w/ derived species	Meteorological conditions and/or relevant notes	Median $ssNa^+$ ($\mu g\ m^{-3}$)	Median Na^+_{dust} ($\mu g\ m^{-3}$)	Median Na^+_{comb} ($\mu g\ m^{-3}$)	Median $ssCa^{2+}$ ($\mu g\ m^{-3}$)	Median Ca^{2+}_{dust} ($\mu g\ m^{-3}$)	Median ssK^+ ($\mu g\ m^{-3}$)	Median K^+_{dust} ($\mu g\ m^{-3}$)	Median K^+_{comb} ($\mu g\ m^{-3}$)
Dec-Feb	30 November 2021	94	7	1	Remains of post-frontal conditions	0.16	0.00	0.00	0.01	0.40	0.01	0.06	0.00
	01 December 2021	95	16	14	Prefrontal, high pressure; smoke in boundary layer near coast	0.35	0.00	0.00	0.01	0.47	0.01	0.05	0.00
	07 December 2021	96	5	3	Postfrontal, cold high pressure behind a strong cold front	0.19	0.00	0.00	0.01	0.22	0.01	0.02	0.00
	11 January 2022	100, 101	6	3	Cold high pressure, cold air outbreak (CAO) conditions	0.36	0.00	0.00	0.01	0.08	0.01	0.01	0.00
	12 January 2022	102, 103	33	11	Cold high pressure	0.16	0.00	0.00	0.01	0.08	0.00	0.03	0.00
	15 January 2022	104	3	2	Postfrontal	0.69	0.00	0.00	0.01	0.04	0.01	0.00	0.00
	18 January 2022	105	11	0	Low pressure moves offshore, sets up CAO conditions	NaN	NaN	NaN	NaN	NaN	NaN	NaN	NaN
	19 January 2022	107, 108	26	6	Short-lived high pressure	0.00	0.01	0.19	0.00	0.07	0.00	0.06	0.06
	24 January 2022	109, 110	26	9	Postfrontal, weak high pressure	0.07	0.00	0.06	0.00	0.09	0.00	0.05	0.02
	26 January 2022	111, 112	20	7	Postfrontal	0.00	0.00	0.37	0.00	0.05	0.00	0.05	0.35
	27 January 2022	113, 114	18	4	Cold high pressure	0.28	0.00	0.00	0.01	0.00	0.01	0.00	0.00
	01 February 2022	115	8	4	High pressure	1.10	0.00	0.00	0.02	0.03	0.02	0.00	0.00
	02 February 2022	116	17	4	High pressure	0.72	0.00	0.00	0.02	0.01	0.02	0.00	0.02

	03 February 2022	117, 118	15	4	High pressure	1.16	0.00	0.00	0.03	0.00	0.04	0.00	0.01
	15 February 2022	120, 121	34	7	Postfrontal conditions, cold high pressure	0.31	0.00	0.00	0.01	0.13	0.01	0.01	0.00
	16 February 2022	122, 123	21	10	Cold high pressure	0.16	0.00	0.00	0.01	0.12	0.00	0.03	0.00
	19 February 2022	124, 125	38	18	Weak postfrontal	0.04	0.00	0.00	0.00	0.11	0.00	0.04	0.00
	22 February 2022	126, 127	25	20	Prefrontal, high pressure	1.73	0.00	0.00	0.05	0.07	0.04	0.00	0.00
	26 February 2022	128, 129	16	14	Postfrontal	0.08	0.00	0.00	0.00	0.05	0.00	0.04	0.00
	Overall		**345**	**141**		**0.20**	**0.00**	**0.00**	**0.01**	**0.08**	**0.01**	**0.03**	**0.00**
	02 March 2022	130	39	30	Postfrontal, high pressure	0.22	0.00	0.00	0.01	0.17	0.00	0.01	0.00
	03 March 2022	131, 132	71	53	Weak prefrontal	0.83	0.00	0.00	0.03	0.26	0.03	0.03	0.00
	04 March 2022	133, 134	42	29	Cold high pressure	1.51	0.00	0.00	0.06	0.05	0.05	0.01	0.00
	13 March 2022	138	8	2	Postfrontal, CAO conditions	0.11	0.00	0.00	0.00	0.59	0.00	0.08	0.00
	14 March 2022	139, 140	38	32	Late postfrontal, cold high pressure; smoke plume sampled from a woodland fire	0.06	0.00	0.01	0.00	0.06	0.00	0.04	0.01
Mar	18 March 2022	141	14	12	Weak postfrontal	0.00	0.00	0.12	0.00	0.04	0.00	0.04	0.07
	26 March 2022	144, 145	29	15	Postfrontal; sampled dust, smoke, and potentially pollen	0.02	0.00	0.01	0.00	0.05	0.00	0.04	0.01
	28 March 2022	146	17	10	Postfrontal	0.07	0.00	0.00	0.00	0.06	0.00	0.04	0.00
	29 March 2022	147, 148	19	4	Postfrontal, high pressure, CAO conditions	0.13	0.00	0.04	0.00	0.15	0.00	0.05	0.02
	Overall		**277**	**187**		**0.18**	**0.00**	**0.00**	**0.01**	**0.12**	**0.01**	**0.03**	**0.00**
May	03 May 2022	149	15	10	Weak prefrontal; presence of smoke potentially from New Mexico	0.39	0.00	0.00	0.01	0.14	0.01	0.05	0.00

	05 May 2022	150, 151	18	9	Postfrontal	0.02	0.00	0.00	0.00	0.05	0.00	0.03	0.00
	16 May 2022	153, 154	39	5	Prefrontal to an approaching cold front yet also postfrontal to a departing band of precipitation	0.29	0.00	0.00	0.01	0.31	0.01	0.02	0.00
	17 May 2022	155	37	2	Postfrontal	0.06	0.00	0.00	0.00	0.01	0.00	0.01	0.00
	20 May 2022	158	28	19	Warm high pressure, southerly flow due to Bermuda high[2]; haze with potential sampling of bioaerosol	2.24	0.00	0.00	0.08	0.06	0.06	0.00	0.00
	Overall		**137**	**45**		**0.42**	**0.00**	**0.00**	**0.01**	**0.08**	**0.01**	**0.01**	**0.00**
Mar transit	22 March 2022	142, 143	48	47	High pressure, two days after a cold front and two days before another cold front	0.45	0.00	0.00	0.02	0.10	0.01	0.05	0.00
	18 May 2022	156, 157	67	23	Postfrontal along East Coast, aircraft passed across the cold front on the way to Bermuda	1.11	0.00	0.00	0.04	0.01	0.02	0.00	0.00
May transit	21 May 2022	159, 160	42	14	Warm high pressure, anticyclonic flow around Bermuda high	1.14	0.00	0.00	0.04	0.01	0.03	0.00	0.00
	31 May 2022	161	11	1	Postfrontal	0.00	0.00	0.20	0.00	0.02	0.00	0.02	0.20
	Overall		**120**	**38**		**1.08**	**0.00**	**0.00**	**0.04**	**0.01**	**0.02**	**0.00**	**0.00**
	02 June 2022	162, 163	4	1	Prefrontal	0.56	0.00	0.27	0.02	0.01	0.02	0.01	0.13
	03 June 2022	164	1	0	Prefrontal, tropical system approaching from the southwest	NaN	NaN	NaN	NaN	NaN	NaN	NaN	NaN
Jun Bermuda	05 June 2022	165	29	24	Could only fly in the morning due to approaching tropical cyclone (TC), TC departs 06 June 2022.	1.94	0.00	0.00	0.07	0.00	0.06	0.00	0.00
	07 June 2022	167	1	0	High behind departing TC	NaN	NaN	NaN	NaN	NaN	NaN	NaN	NaN
	08 June 2022	168, 169	2	1	High pressure behind TC, African dust known to be in domain	0.00	0.18	5.94	0.00	1.07	0.00	1.08	1.96

	10 June 2022	170	1	1	High pressure, isolated thunderstorms, African dust known to be in domain	2.28	0.00	0.00	0.06	0.00	0.01	0.00	0.00
	11 June 2022	172, 173	20	7	High pressure, African dust known to be in domain	0.89	0.00	0.00	0.03	0.19	0.03	0.01	0.00
	13 June 2022	174	25	17	High pressure, African dust known to be in domain but sampled away from dust for contrast	1.38	0.00	0.00	0.05	0.00	0.04	0.00	0.00
	Overall		**83**	**51**		**1.34**	**0.00**	**0.00**	**0.05**	**0.01**	**0.04**	**0.00**	**0.00**

[1]Davis et al. (1997)

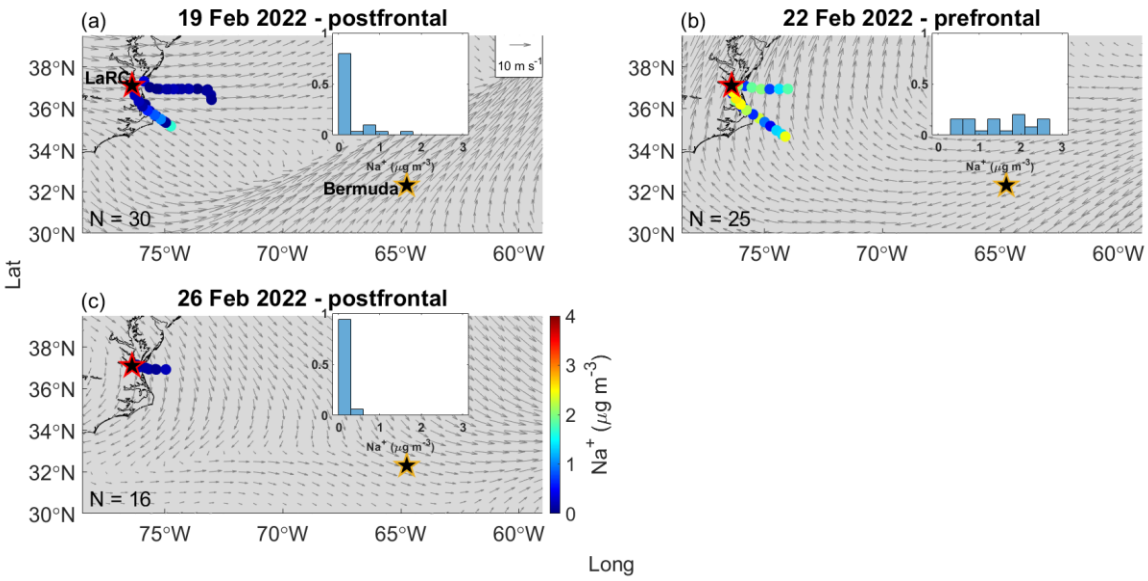

160

161 **Figure S1.** Bulk PILS Na^+ mass concentrations from clear ensembles during flights experiencing
162 (**a**) postfrontal conditions on 19 February 2022 (RFs 124 and 125) (**b**) prefrontal conditions on
163 22 February 2022 (RFs 126 and 127), and (**c**) postfrontal conditions on 26 February 2022 (RFs
164 128 and 129). NASA Langley Research Center (LaRC) and Bermuda are marked with red-edged
165 and gold-edged stars, respectively. Normalized histograms in each panel show the distribution of
166 bulk PILS Na^+ mass concentrations for the date indicated since overlap among the colored dots
167 can hide some from view. Grey arrows in each panel indicate the average magnitude and
168 direction of winds at 950 hPa from MERRA-2 at 3-hour time resolution during periods relevant
169 to each RF.

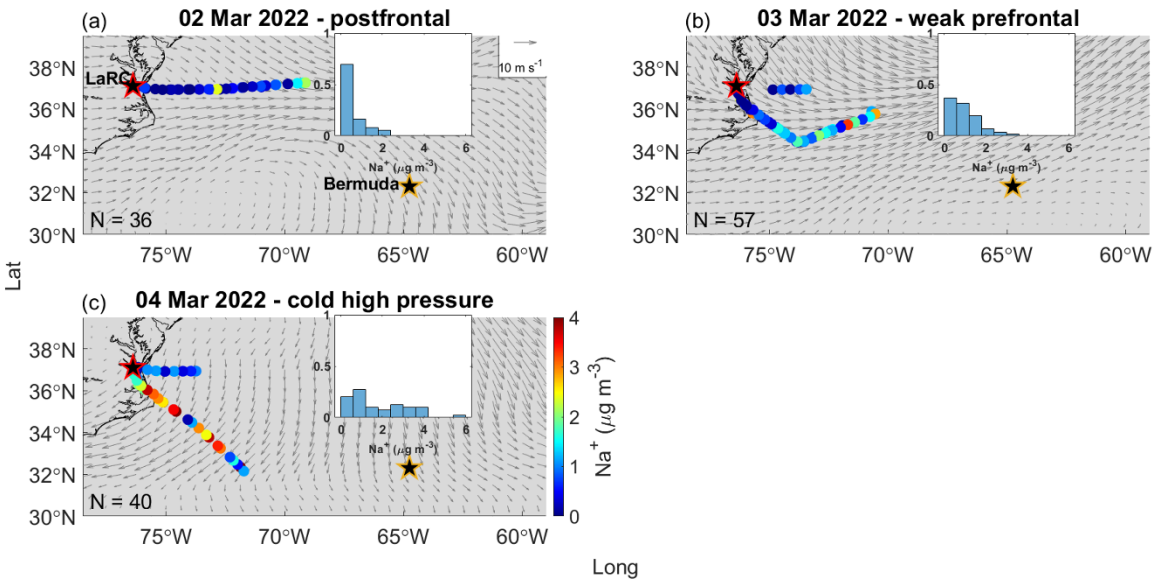

Figure S2. Same as Fig. S1 except for (**a**) postfrontal conditions on 02 March 2022 (RF 130), (**b**) weak prefrontal conditions on 03 March 2022 (RFs 131 and 132), and (**c**) cold high pressure on 04 March 2022 (RFs 133 and 134).

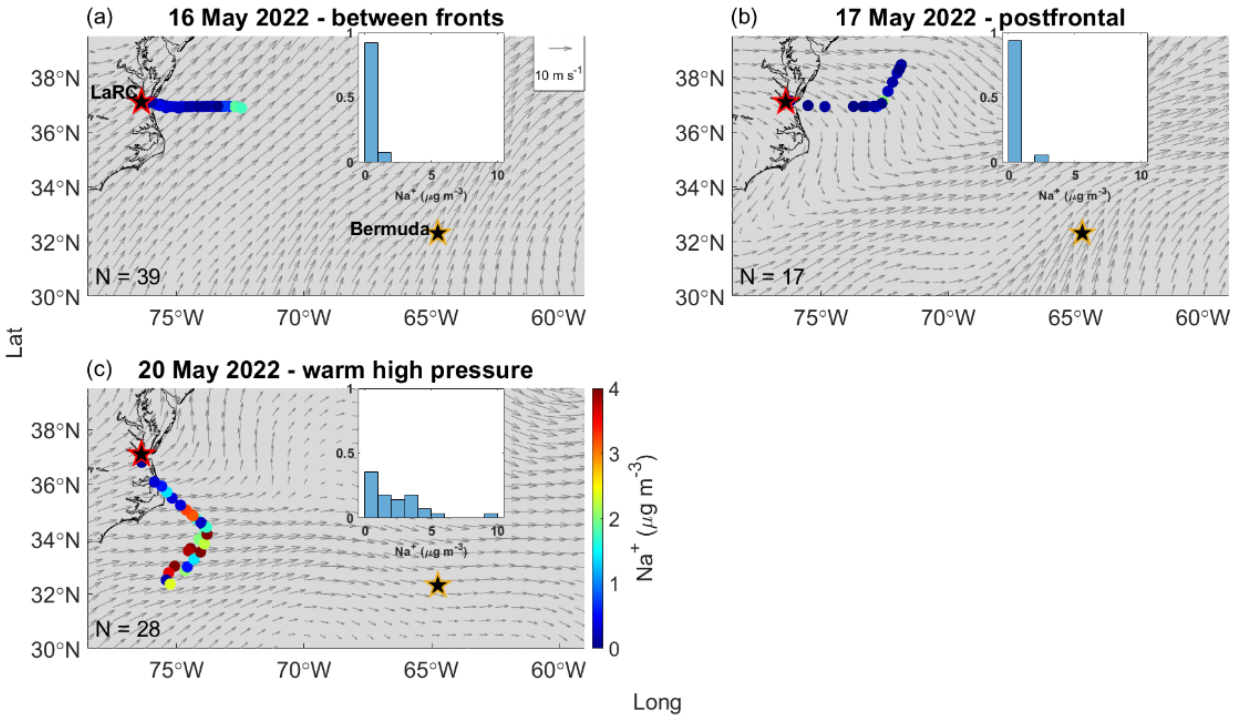

174

175 **Figure S3.** Same as Fig. S1 except for (**a**) conditions between fronts on 16 May 2022 (RFs 153
176 and 154), (**b**) postfrontal conditions on 17 May 2022 (RF 155), and (**c**) warm high pressure on 20
177 May 2022 (RF 158).

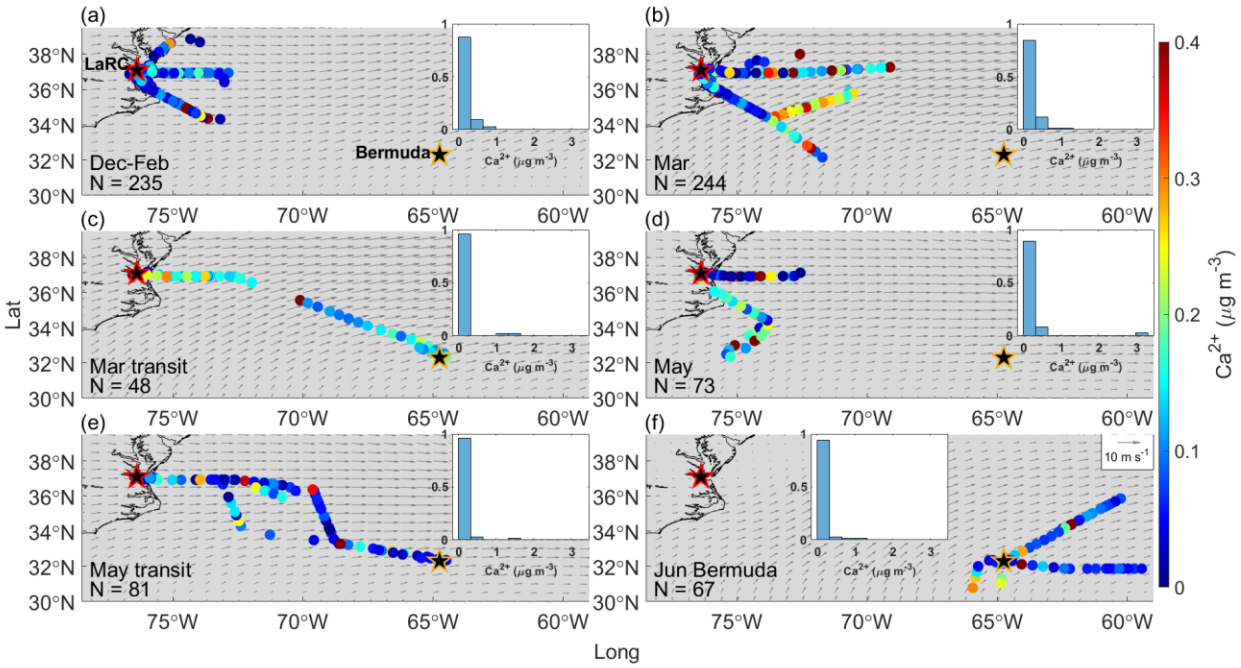

Figure S4. Bulk PILS Ca^{2+} mass concentrations from clear ensembles during (**a**) December 2021-February 2022, (**b**) March 2022, (**c**) March 2022 transit flights between LaRC (marked with a red-edged star) and Bermuda (marked with a golden-edged star), (**d**) May 2022, (**e**) May 2022 transit flights between LaRC and Bermuda, and (**f**) the Bermuda field campaign in June 2022. Normalized histograms in each panel show the distribution of bulk PILS Ca^{2+} mass concentrations for that specific category since overlap among the colored dots can hide some from view. Grey arrows indicate the average magnitude and direction of MERRA-2 winds at 950 hPa for the month(s) relevant to each category.

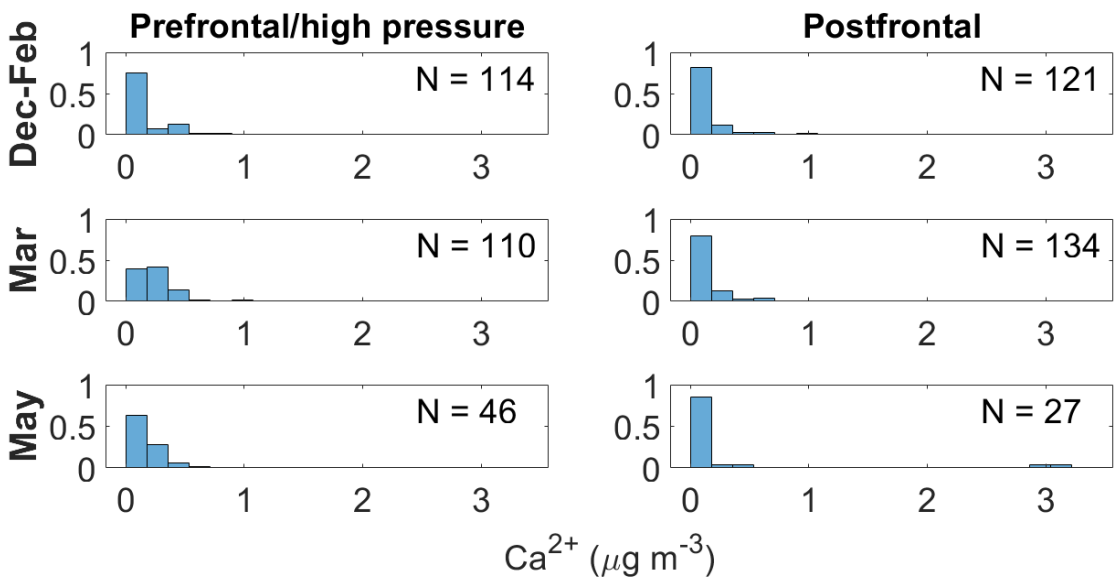

187

188 **Figure S5.** Normalized histograms showing differences in bulk PILS Ca^{2+} mass concentration
189 from clear ensembles occurring in prefrontal and/or high-pressure versus postfrontal conditions
190 for December-February (top row), March (middle row), and May (bottom row). These categories
191 are shown as they represent flights occurring in and around the East Coast, eliminating coastal
192 versus open-ocean sampling as a confounding variable.

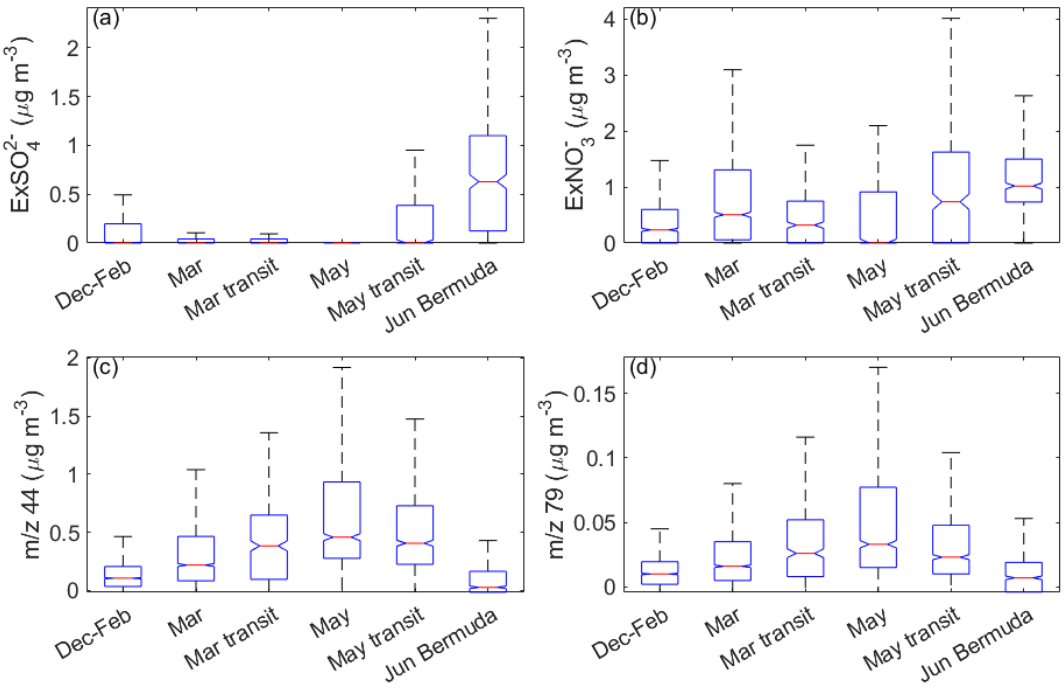

193

194 **Figure S6.** Notched box plots showing seasonal/categorical differences in mass concentrations
195 from clear ensembles of (**a**) excess SO_4^{2-} ($ExSO_4^{2-}$), (**b**) excess NO_3^- ($ExNO_3^-$), and spectral
196 markers for (**c**) oxygenated organics, *m/z* 44, and (**d**) methanesulfonic acid (MSA), *m/z* 79.

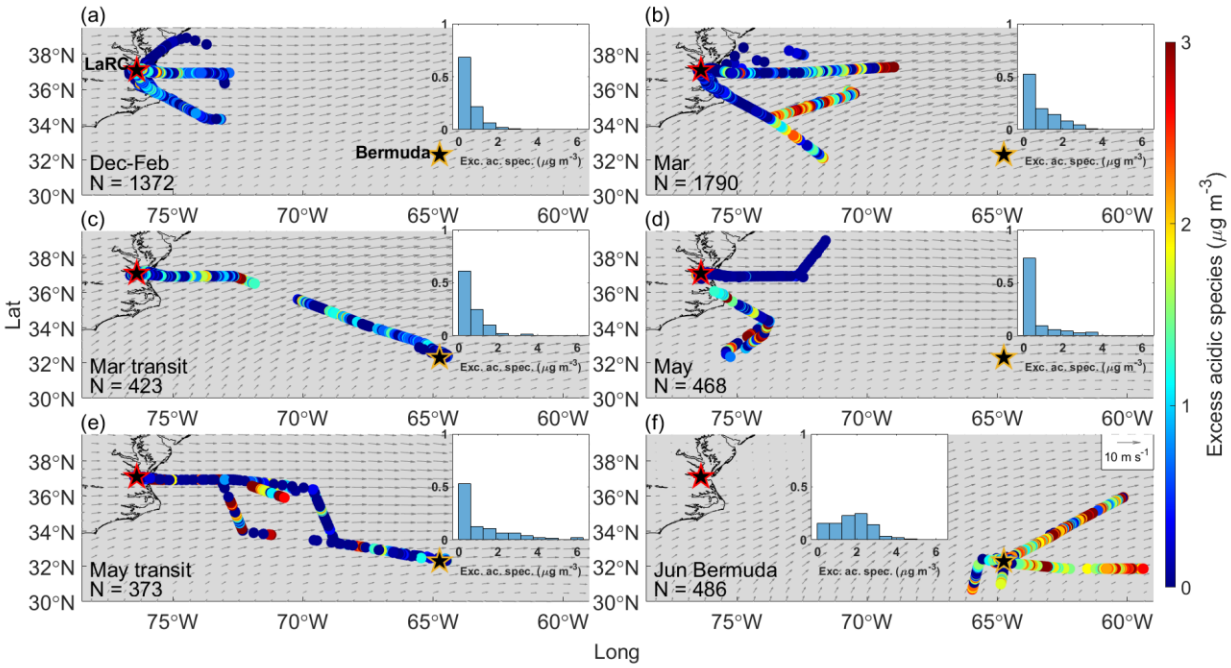

197

198 **Figure S7.** Same as Fig. S4, except for derived mass concentrations of excess acidic species.

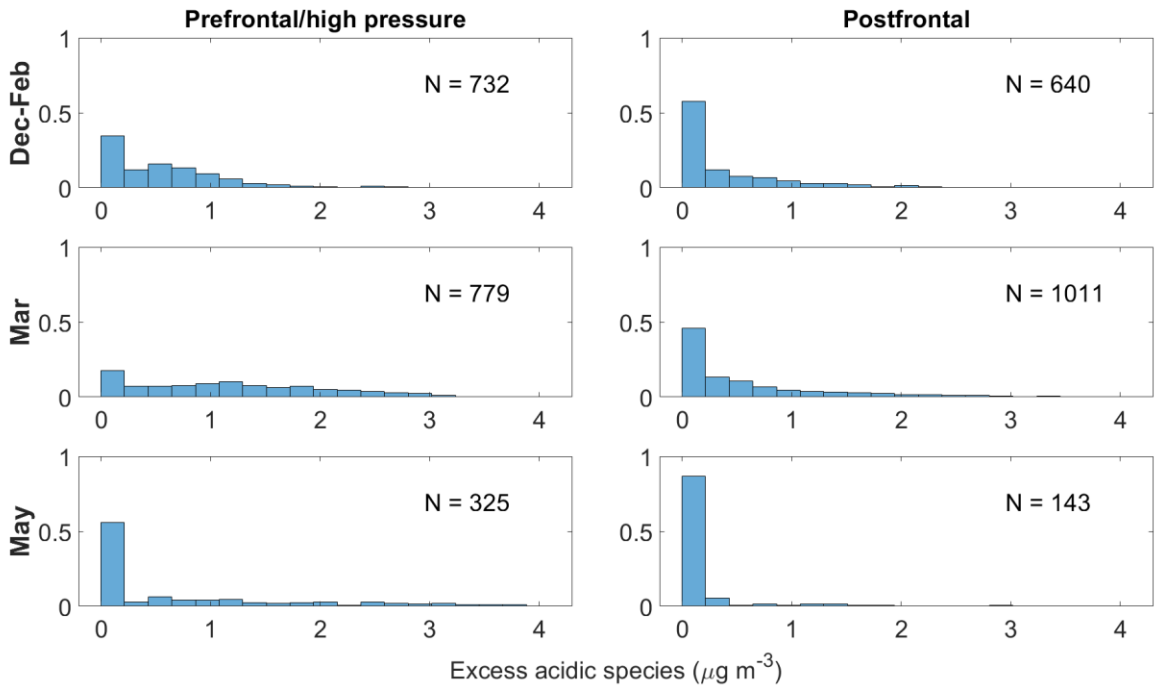

Figure S8. Same as Fig. S5, except for mass concentrations of excess acidic species.

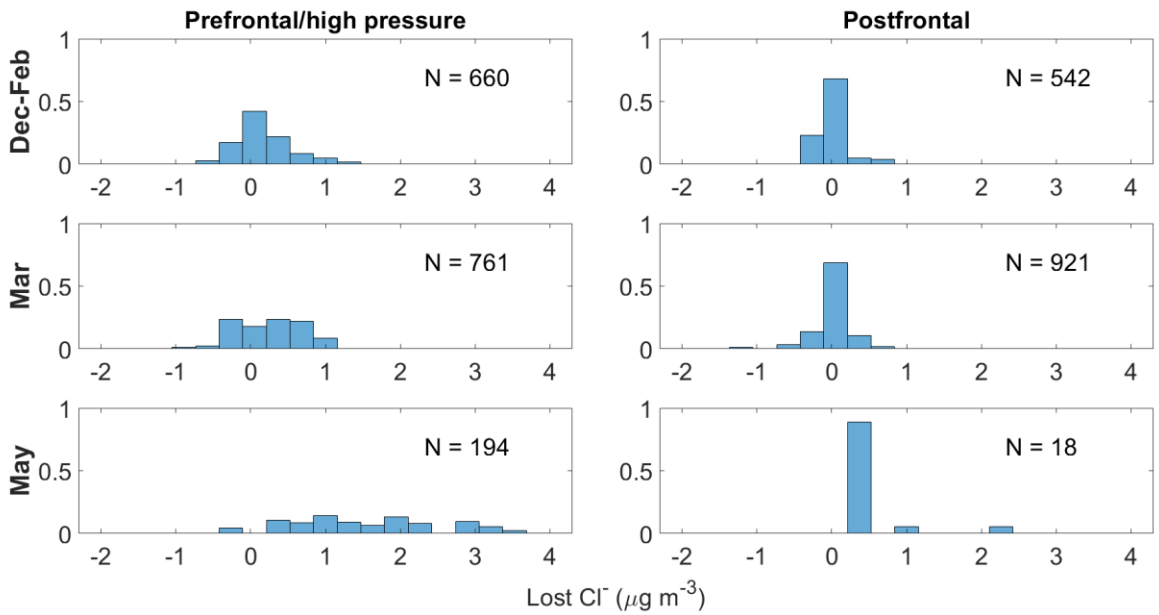

Figure S9. Same as Fig. S5, except for lost Cl^- mass concentration.

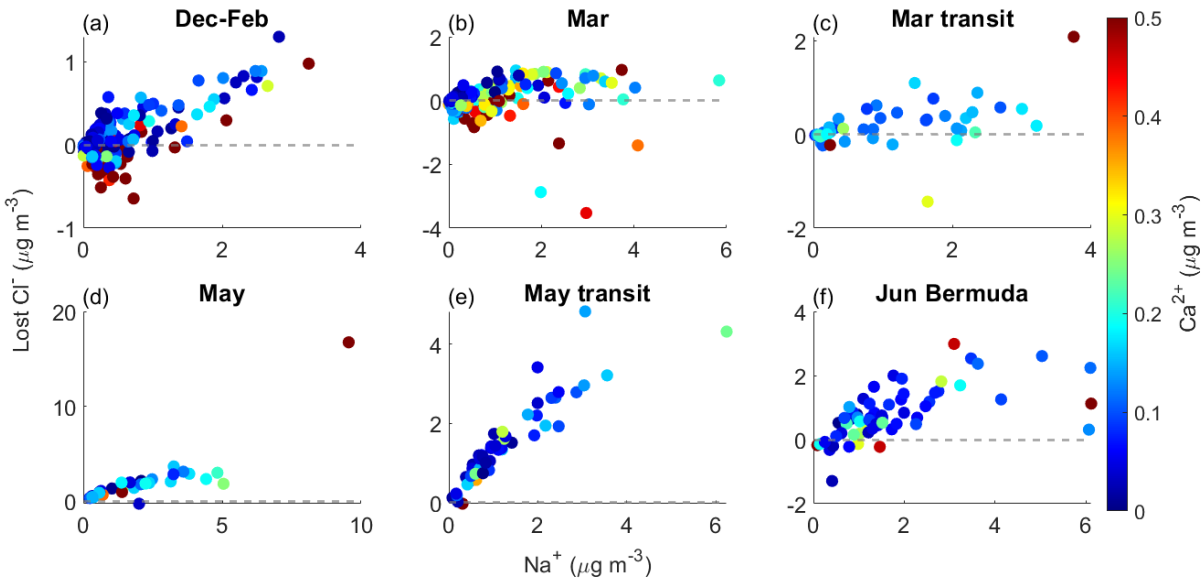

Figure S10. Relationships between mass concentration of bulk PILS Na^+ and lost Cl^- colored by bulk PILS Ca^{2+} mass concentration for the (**a**) December-February, (**b**) March, (**c**) March transit, (**d**) May, (**e**) May transit, and (**f**) June Bermuda categories.

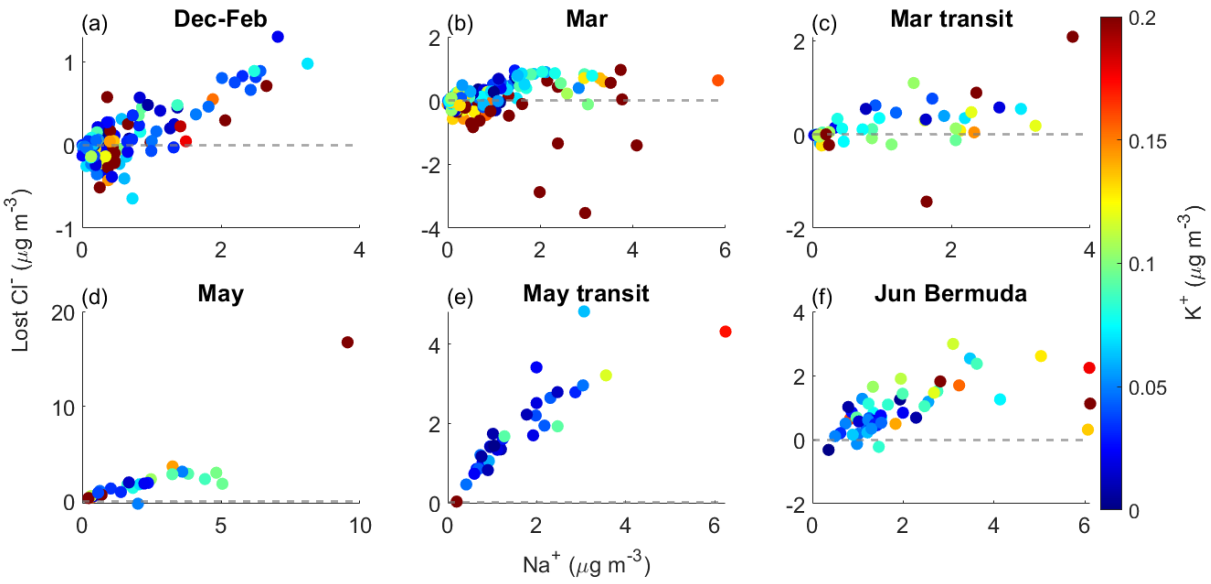

207

208 **Figure S11.** Same as Fig. S10, except colored by bulk PILS K^+ mass concentration.

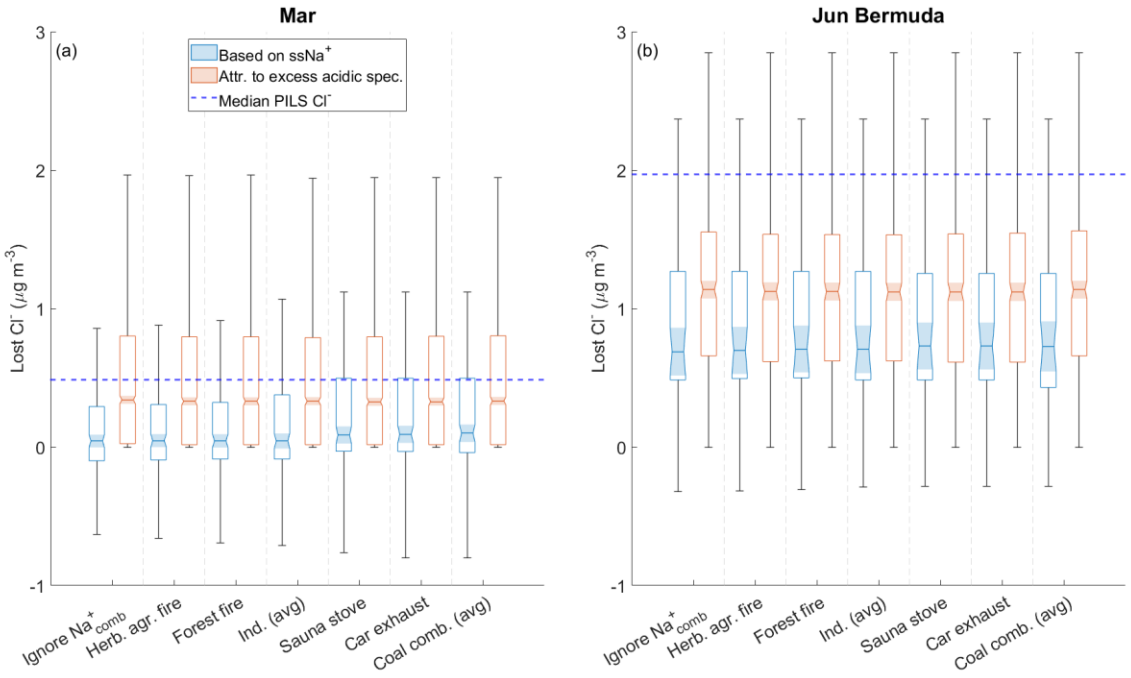

Figure S12. Notched box plots showing the sensitivity in actual and theoretical lost Cl^- to accounting for Na^+ from dust and various combustion processes during flights in (**a**) March near the East Coast and (**b**) during the June field campaign in Bermuda. Light blue boxes represent the actual Cl^- displaced from sea salt particles based on derived mass concentrations of $ssNa^+$, while light red boxes represent the theoretical Cl^- that could have been displaced by the derived mass concentrations of excess acidic species. Combustion processes were assumed to not contribute to bulk PILS Na^+ mass concentrations for the "Ignore Na^+_{comb}" results represented by the pair of boxes farthest to the left in each panel. The remaining pairs of boxes are for the Na^+:K^+ ratios described in Table S3 used to derive actual and theoretical lost Cl^-. Note that "Herb. agr. fire" above stands for "Herbaceous agricultural fire." The solid red line in the center of each box indicates the median, box edges represent the 25th and 75th percentiles, and the lower and upper whiskers indicate the lower limit (first quartile – 1.5 × interquartile range) and upper limit (third quartile + 1.5 × interquartile range), respectively. The notches span the 95th confidence interval for the median. The horizontal dashed blue lines indicate the median bulk PILS Cl^- mass concentration for each category.

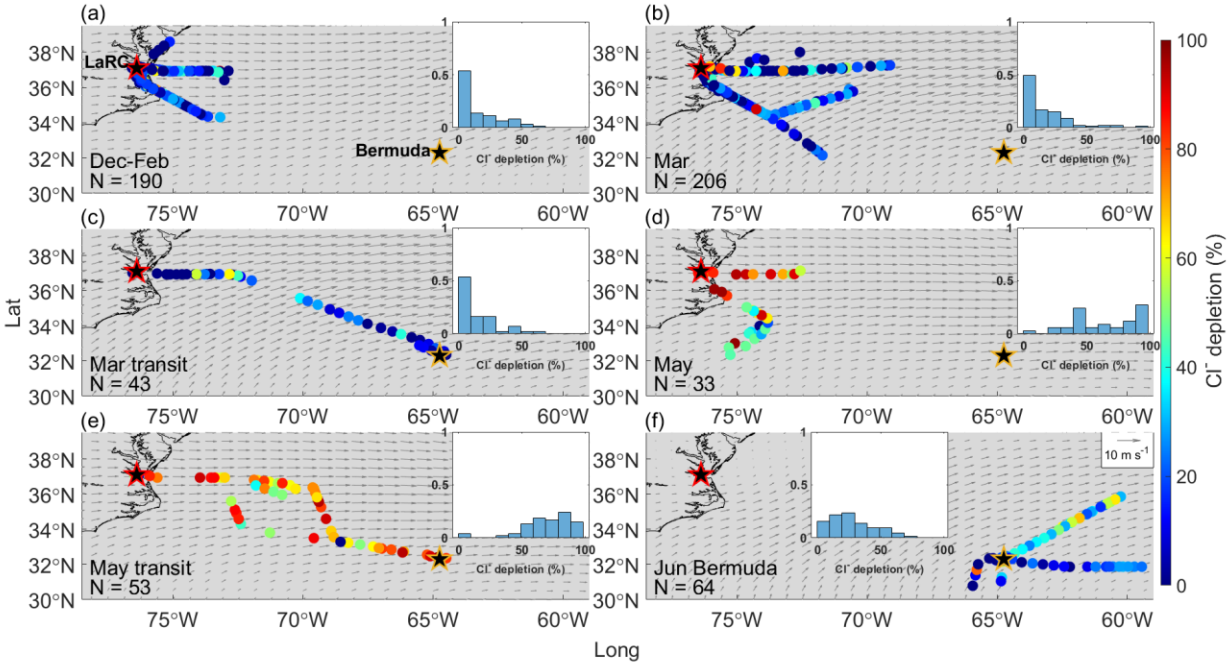

Figure S13. Same as Fig. S4, except for %Cl^- depletion.

References

Aldhaif, A. M., Lopez, D. H., Dadashazar, H., and Sorooshian, A.: Sources, frequency, and chemical nature of dust events impacting the United States East Coast, Atmospheric Environment, 231, 117456, https://doi.org/10.1016/j.atmosenv.2020.117456, 2020.

AzadiAghdam, M., Braun, R. A., Edwards, E.-L., Bañaga, P. A., Cruz, M. T., Betito, G., Cambaliza, M. O., Dadashazar, H., Lorenzo, G. R., Ma, L., MacDonald, A. B., Nguyen, P., Simpas, J. B., Stahl, C., and Sorooshian, A.: On the nature of sea salt aerosol at a coastal megacity: Insights from Manila, Philippines in Southeast Asia, Atmospheric Environment, 216, 116922, https://doi.org/10.1016/j.atmosenv.2019.116922, 2019.

Becagli, S., Proposito, M., Benassai, S., Gragnani, R., Magand, O., Traversi, R., and Udisti, R.: Spatial distribution of biogenic sulphur compounds (MSA, nssSO42–) in the northern Victoria Land–Dome C–Wilkes Land area, East Antarctica, Annals of Glaciology, 41, 23–31, https://doi.org/10.3189/172756405781813384, 2005.

Bondy, A. L., Wang, B., Laskin, A., Craig, R. L., Nhliziyo, M. V., Bertman, S. B., Pratt, K. A., Shepson, P. B., and Ault, A. P.: Inland Sea Spray Aerosol Transport and Incomplete Chloride Depletion: Varying Degrees of Reactive Processing Observed during SOAS, Environ. Sci. Technol., 51, 9533–9542, https://doi.org/10.1021/acs.est.7b02085, 2017.

Boreddy, S. K. R. and Kawamura, K.: A 12-year observation of water-soluble ions in TSP aerosols collected at a remote marine location in the western North Pacific: an outflow region of Asian dust, Atmospheric Chemistry and Physics, 15, 6437–6453, https://doi.org/10.5194/acp-15-6437-2015, 2015.

Bowen, H. J. M.: Environmental chemistry of the elements, Academic Press, London, New York, xv, 333 pp., 1979.

Corral, A. F., Braun, R. A., Cairns, B., Gorooh, V. A., Liu, H., Ma, L., Mardi, A. H., Painemal, D., Stamnes, S., van Diedenhoven, B., Wang, H., Yang, Y., Zhang, B., and Sorooshian, A.: An Overview of Atmospheric Features Over the Western North Atlantic Ocean and North American East Coast – Part 1: Analysis of Aerosols, Gases, and Wet Deposition Chemistry, Journal of Geophysical Research: Atmospheres, 126, e2020JD032592, https://doi.org/10.1029/2020JD032592, 2021.

Davis, R. E., Hayden, B. P., Gay, D. A., Phillips, W. L., and Jones, G. V.: The North Atlantic Subtropical Anticyclone, Journal of Climate, 10, 728–744, https://doi.org/10.1175/1520-0442(1997)010<0728:TNASA>2.0.CO;2, 1997.

Farren, N. J., Dunmore, R. E., Mead, M. I., Mohd Nadzir, M. S., Samah, A. A., Phang, S.-M., Bandy, B. J., Sturges, W. T., and Hamilton, J. F.: Chemical characterisation of water-soluble ions in atmospheric particulate matter on the east coast of Peninsular Malaysia, Atmospheric Chemistry and Physics, 19, 1537–1553, https://doi.org/10.5194/acp-19-1537-2019, 2019.

Feng, L., Shen, H., Zhu, Y., Gao, H., and Yao, X.: Insight into Generation and Evolution of Sea-Salt Aerosols from Field Measurements in Diversified Marine and Coastal Atmospheres, Scientific Reports, 7, 41260, https://doi.org/10.1038/srep41260, 2017.

Finlayson-Pitts, B. J. and Pitts, J. N.: CHAPTER 9 - Particles in the Troposphere, in: Chemistry of the Upper and Lower Atmosphere, edited by: Finlayson-Pitts, B. J. and Pitts, J. N., Academic Press, San Diego, 349–435, https://doi.org/10.1016/B978-012257060-5/50011-3, 2000.

Haskins, J. D., Jaeglé, L., Shah, V., Lee, B. H., Lopez-Hilfiker, F. D., Campuzano-Jost, P., Schroder, J. C., Day, D. A., Guo, H., Sullivan, A. P., Weber, R., Dibb, J., Campos, T., Jimenez, J. L., Brown, S. S., and Thornton, J. A.: Wintertime Gas-Particle Partitioning and Speciation of Inorganic Chlorine in the Lower Troposphere Over the Northeast United States and Coastal Ocean, Journal of Geophysical Research: Atmospheres, 123, 12,897-12,916, https://doi.org/10.1029/2018JD028786, 2018.

Heintzenberg, J., Covert, D. C., and Dingenen, R. V.: Size distribution and chemical composition of marine aerosols: a compilation and review, Tellus B: Chemical and Physical Meteorology, 52, 1104–1122, https://doi.org/10.3402/tellusb.v52i4.17090, 2000.

Holland, H. D.: The chemistry of the atmosphere and oceans, New York : Wiley, 378 pp., 1978.

Huang, X., Olmez, I., Aras, N. K., and Gordon, G. E.: Emissions of trace elements from motor vehicles: Potential marker elements and source composition profile, Atmospheric Environment, 28, 1385–1391, https://doi.org/10.1016/1352-2310(94)90201-1, 1994.

Jiang, B., Xie, Z., Lam, P. K. S., He, P., Yue, F., Wang, L., Huang, Y., Kang, H., Yu, X., and Wu, X.: Spatial and Temporal Distribution of Sea Salt Aerosol Mass Concentrations in the Marine Boundary Layer From the Arctic to the Antarctic, Journal of Geophysical Research: Atmospheres, 126, e2020JD033892, https://doi.org/10.1029/2020JD033892, 2021.

Junge, C. E. and Werby, R. T.: THE CONCENTRATION OF CHLORIDE, SODIUM, POTASSIUM, CALCIUM, AND SULFATE IN RAIN WATER OVER THE UNITED STATES, Journal of the Atmospheric Sciences, 15, 417–425, https://doi.org/10.1175/1520-0469(1958)015<0417:TCOCSP>2.0.CO;2, 1958.

Keene, W. C. and Savoie, D. L.: The pH of deliquesced sea-salt aerosol in polluted marine air, Geophysical Research Letters, 25, 2181–2184, https://doi.org/10.1029/98GL01591, 1998.

Keene, W. C., Pszenny, A. A. P., Galloway, J. N., and Hawley, M. E.: Sea-salt corrections and interpretation of constituent ratios in marine precipitation, Journal of Geophysical Research: Atmospheres, 91, 6647–6658, https://doi.org/10.1029/JD091iD06p06647, 1986.

Keene, W. C., Pszenny, A. A. P., Jacob, D. J., Duce, R. A., Galloway, J. N., Schultz-Tokos, J. J., Sievering, H., and Boatman, J. F.: The geochemical cycling of reactive chlorine through the marine troposphere, Global Biogeochemical Cycles, 4, 407–430, https://doi.org/10.1029/GB004i004p00407, 1990.

299 Keene, W. C., Pszenny, A. A. P., Maben, J. R., Stevenson, E., and Wall, A.: Closure evaluation
300 of size-resolved aerosol pH in the New England coastal atmosphere during summer, Journal of
301 Geophysical Research: Atmospheres, 109, D23307, https://doi.org/10.1029/2004JD004801,
302 2004.

303 Keene, W. C., Stutz, J., Pszenny, A. A. P., Maben, J. R., Fischer, E. V., Smith, A. M., von
304 Glasow, R., Pechtl, S., Sive, B. C., and Varner, R. K.: Inorganic chlorine and bromine in coastal
305 New England air during summer, Journal of Geophysical Research: Atmospheres, 112, D10S12,
306 https://doi.org/10.1029/2006JD007689, 2007.

307 Klopper, D., Formenti, P., Namwoonde, A., Cazaunau, M., Chevaillier, S., Feron, A., Gaimoz,
308 C., Hease, P., Lahmidi, F., Mirande-Bret, C., Triquet, S., Zeng, Z., and Piketh, S. J.: Chemical
309 composition and source apportionment of atmospheric aerosols on the Namibian coast,
310 Atmospheric Chemistry and Physics, 20, 15811–15833, https://doi.org/10.5194/acp-20-15811-
311 2020, 2020.

312 Lamberg, H., Nuutinen, K., Tissari, J., Ruusunen, J., Yli-Pirilä, P., Sippula, O., Tapanainen, M.,
313 Jalava, P., Makkonen, U., Teinilä, K., Saarnio, K., Hillamo, R., Hirvonen, M.-R., and Jokiniemi,
314 J.: Physicochemical characterization of fine particles from small-scale wood combustion,
315 Atmospheric Environment, 45, 7635–7643, https://doi.org/10.1016/j.atmosenv.2011.02.072,
316 2011.

317 Manders, A. M. M., Schaap, M., Querol, X., Albert, M. F. M. A., Vercauteren, J., Kuhlbusch, T.
318 A. J., and Hoogerbrugge, R.: Sea salt concentrations across the European continent, Atmospheric
319 Environment, 44, 2434–2442, https://doi.org/10.1016/j.atmosenv.2010.03.028, 2010.

320 Murphy, D. M., Froyd, K. D., Bian, H., Brock, C. A., Dibb, J. E., DiGangi, J. P., Diskin, G.,
321 Dollner, M., Kupc, A., Scheuer, E. M., Schill, G. P., Weinzierl, B., Williamson, C. J., and Yu, P.:
322 The distribution of sea-salt aerosol in the global troposphere, Atmospheric Chemistry and
323 Physics, 19, 4093–4104, https://doi.org/10.5194/acp-19-4093-2019, 2019.

324 Nolte, C., Bhave, P., Arnold, J., Dennis, R., Zhang, K., and Wexler, A.: Modeling urban and
325 regional aerosols—Application of the CMAQ-UCD Aerosol Model to Tampa, a coastal urban
326 site, Atmospheric Environment, 42, 3179–3191, https://doi.org/10.1016/j.atmosenv.2007.12.059,
327 2008.

328 Ondov, J. M., Choquette, C. E., Zoller, W. H., Gordon, G. E., Biermann, A. H., and Heft, R. E.:
329 Atmospheric behavior of trace elements on particles emitted from a coal-fired power plant,
330 Atmospheric Environment, 23, 2193–2204, https://doi.org/10.1016/0004-6981(89)90181-9,
331 1989.

332 Ooki, A., Uematsu, M., Miura, K., and Nakae, S.: Sources of sodium in atmospheric fine
333 particles, Atmospheric Environment, 36, 4367–4374, https://doi.org/10.1016/S1352-
334 2310(02)00341-2, 2002.

335 Pilson, M. E. Q.: An Introduction to the Chemistry of the Sea, 1st ed., Prentice Hall, 1998.

Prospero, J. M.: Mineral and sea salt aerosol concentrations in various ocean regions, Journal of Geophysical Research: Oceans, 84, 725–731, https://doi.org/10.1029/JC084iC02p00725, 1979.

Quinn, P. K. and Bates, T. S.: Regional aerosol properties: Comparisons of boundary layer measurements from ACE 1, ACE 2, Aerosols99, INDOEX, ACE Asia, TARFOX, and NEAQS, Journal of Geophysical Research: Atmospheres, 110, D14202, https://doi.org/10.1029/2004JD004755, 2005.

Quinn, P. K., Coffman, D. J., Bates, T. S., Miller, T. L., Johnson, J. E., Voss, K., Welton, E. J., and Neusüss, C.: Dominant aerosol chemical components and their contribution to extinction during the Aerosols99 cruise across the Atlantic, Journal of Geophysical Research: Atmospheres, 106, 20783–20809, https://doi.org/10.1029/2000JD900577, 2001.

Riley, J. P. and Chester, R. (Eds.): Copyright, in: Chemical Oceanography (Second Edition), Academic Press, iv, https://doi.org/10.1016/B978-0-12-588606-2.50002-3, 1976.

Scheff, P. A. and Valiozis, C.: Characterization and source identification of respirable particulate matter in Athens, Greece, Atmospheric Environment. Part A. General Topics, 24, 203–211, https://doi.org/10.1016/0960-1686(90)90457-X, 1990.

Seinfeld, J. H. and Pandis, S. N.: Atmospheric Chemistry and Physics: From Air Pollution to Climate Change, John Wiley & Sons, 1146 pp., 2016.

Shinozuka, Y., Clarke, A. D., Howell, S. G., Kapustin, V. N., and Huebert, B. J.: Sea-salt vertical profiles over the Southern and tropical Pacific oceans: Microphysics, optical properties, spatial variability, and variations with wind speed, Journal of Geophysical Research: Atmospheres, 109, D24201, https://doi.org/10.1029/2004JD004975, 2004.

Spada, M., Jorba, O., Pérez García-Pando, C., Janjic, Z., and Baldasano, J. M.: On the evaluation of global sea-salt aerosol models at coastal/orographic sites, Atmospheric Environment, 101, 41–48, https://doi.org/10.1016/j.atmosenv.2014.11.019, 2015.

Stumm, W. and Morgan, J. J. aut: Aquatic chemistry : an introd. emphasizing chemical equilibria in natural waters, New York [u.a.] : Wiley, 804 pp., 1981.

Turn, S. Q., Jenkins, B. M., Chow, J. C., Pritchett, L. C., Campbell, D., Cahill, T., and Whalen, S. A.: Elemental characterization of particulate matter emitted from biomass burning: Wind tunnel derived source profiles for herbaceous and wood fuels, Journal of Geophysical Research: Atmospheres, 102, 3683–3699, https://doi.org/10.1029/96JD02979, 1997.

Wai, K.-M. and Tanner, P. A.: Wind-dependent sea salt aerosol in a Western Pacific coastal area, Atmospheric Environment, 38, 1167–1171, https://doi.org/10.1016/j.atmosenv.2003.11.007, 2004.

Watson, J. G., Chow, J. C., and Houck, J. E.: PM2.5 chemical source profiles for vehicle exhaust, vegetative burning, geological material, and coal burning in Northwestern Colorado during 1995, Chemosphere, 43, 1141–1151, https://doi.org/10.1016/S0045-6535(00)00171-5, 2001.

Wilson, T. R. S.: Salinity and the major elements of sea water, in: Chemical Oceanography, vol. 1, Academic, Orlando, FL, USA, 365–413, 1975.

Yao, X. and Zhang, L.: Chemical processes in sea-salt chloride depletion observed at a Canadian rural coastal site, Atmospheric Environment, 46, 189–194, https://doi.org/10.1016/j.atmosenv.2011.09.081, 2012.

Zhao, Y. and Gao, Y.: Acidic species and chloride depletion in coarse aerosol particles in the US east coast, Science of The Total Environment, 407, 541–547, https://doi.org/10.1016/j.scitotenv.2008.09.002, 2008.

Zhuang, H., Chan, C. K., Fang, M., and Wexler, A. S.: Formation of nitrate and non-sea-salt sulfate on coarse particles, Atmospheric Environment, 33, 4223–4233, https://doi.org/10.1016/S1352-2310(99)00186-7, 1999.